Rhinovirus Uses a Phosphatidylinositol 4-Phosphate/ Cholesterol Counter-Current for the Formation of Replication Compartments at the ER-Golgi Interface

Pascal S Roulin[1,2], Mark Lötzerich[1], Federico Torta[3], Lukas B Tanner[3,4], Frank JM van Kuppeveld[5], Markus R Wenk[3] and Urs F Greber[1,6]

[1] Institute of Molecular Life Sciences, University of Zurich, Winterthurerstrasse 190, 8057 Zurich, Switzerland

[2] Life Science Zurich Graduate School, Molecular Life Sciences Program, Zurich, Switzerland

[3] Department of Biochemistry, Yong Loo Lin School of Medicine, National University of Singapore, 28 Medical Drive, Singapore 117456, Singapore

[4] presently at: Lewis-Sigler Institute for Integrative Genomics, Princeton University, Washington Road, Princeton, NJ 08544, USA

[5] Virology Division, Department of Infectious Diseases and Immunology, Faculty of Veterinary Medicine, University of Utrecht, 3584CL Utrecht, The Netherlands

[6] corresponding author: E-mail: urs.greber@imls.uzh.ch, Telephone: +41 44 635 48 41, Fax: +41 44 635 68 17

Summary

Similar to other positive-strand RNA viruses, rhinovirus, the causative agent of the common cold, replicates on a web of cytoplasmic membranes, orchestrated by host proteins and lipids. The host pathways that facilitate the formation and function of the replication membranes and complexes are poorly understood. We show that rhinovirus replication depends on host factors driving phosphatidylinositol 4-phosphate (PI4P)-cholesterol counter-currents at viral replication membranes. Depending on the virus type, replication required phosphatidylinositol 4-kinase class 3beta (PI4K3b), cholesteryl-esterase hormone-sensitive lipase (HSL) or oxysterol-binding protein (OSBP)-like 1, 2, 5, 9 or 11 associated with lipid droplets, endosomes or Golgi. Replication invariably required OSBP1, which shuttles cholesterol and PI4P between ER and Golgi at membrane contact sites. Infection also required ER-associated PI4P phosphatase Sac1 and phosphatidylinositol (PI) transfer protein beta (PITPb) shunting PI between ER-Golgi. These data support a PI4P-cholesterol counter-flux model for rhinovirus replication.

Highlights

- Lipid kinase PI4K3b is enriched at rhinovirus replication sites and supports replication
- Lipid droplet-derived cholesterol is enriched on rhinovirus (HRV) replication sites
- Oxysterol-binding protein (OSBP)1 broadly supports enterovirus infections
- Fueled by storage cholesterol, the PI4K3b-OSBP1-Sac1-PITPb cycle drives HRV replication

Roulin et al. present evidence for a lipid counter-current model boosting rhinovirus infection. High concentrations of phosphatidyl-inositol (PI) 4-phosphate are built-up on Golgi membranes and used by oxysterol-binding protein-1, a sterol-dependent transducer in cytokine signaling to load cholesterol onto viral replication membranes at ER-Golgi contact sites using lipid droplet cholesteryl-esters.

Introduction

Human rhinoviruses (HRV) are the causative agents of common colds and have a critical role in exacerbations of asthma, chronic obstructive pulmonary disease and cystic fibrosis (Gern, 2010). They set off severe economic burdens, in part, because there are no approved treatments against rhinovirus infections. HRVs are positive-strand RNA viruses from the *Enterovirus* genus of the *Picornaviridae* family which comprises poliovirus, coxsackievirus (CV), enterovirus or echovirus. Similar to togaviruses, flaviviruses or picornaviruses, they build up membrane-associated replication complexes in the cytoplasm, composed of lipids, viral and cellular proteins and replicating RNA (Belov and van Kuppeveld, 2012). In case of hepaciviruses and picornaviruses, the replication complexes form a tubulo-vesicular network of endomembranes with positive curvature.

There are more than 150 HRV types in three species, HRV-A (74 types), HRV-B (25) and HRV-C (55) (Jacobs et al., 2013). HRV-A and HRV-B types are classified into major and minor groups. They use intercellular adhesion molecule 1 (ICAM1) or low density lipoprotein (LDL) family receptors for entry, respectively. The recently discovered HRV-C types use an unknown receptor, and are difficult to grow in standard tissue culture. Rhinovirus is composed of an icosahedral capsid enclosing a positive-sense single-stranded RNA genome of about 7200 nucleotides. It enters cells by receptor-mediated endocytosis and uncoats upon receiving cues from receptor binding and low pH in endosomes (Suomalainen and Greber, 2013). At 30-60 min after endocytic uptake, viral RNA is uncoated and translated into a polyprotein, which is processed by viral proteases into capsid proteins (viral proteins, VP), membrane associated proteins and replication proteins, including viral RNA polymerase (3Dpol) and proteases 2A and 3C/D. This results in drastic changes in the endomembrane system, in part due to a block in secretion (Sharp and Estes, 2010).

How viral proteins interact with cellular factors and lipids to build up replication membranes is important for both fundamental research and drug development strategies (Heaton and Randall, 2011). For example, phosphatidylinositol (PI) and its phosphorylated derivatives produced by PI kinases (PIK) have key functions in membrane trafficking and signalling. There are two classes of phosphatidylinositol 4-kinases (class 2 and 3 PI4K). Class 3 PI4K has been implicated in replication of hepatitis

C virus and picornaviruses (Hsu et al., 2010; Reiss et al., 2011; Spickler et al., 2013; van der Schaar et al., 2013). PI4K2a effectively functions on endosomes, PI4K2b is involved in the transmission of stress signals, and producing $PI4,5P_2$ at the plasma membrane and other membranes, and PI4K3a has been implicated in the formation of ER exit sites for cargo export from ER to Golgi (Balla, 2013). PI4K3b regulates membrane traffic within the Golgi, and Golgi to plasma membrane transport (Godi et al., 1999). PI4Ks produce PI4P from PI. PI4P effectors at the trans-Golgi-network (TGN) include coat adaptors for vesicular trafficking, such as the clathrin adaptor 1, and γ-ear-containing Arf-binding proteins, and also soluble lipid transfer proteins, such as oxysterol binding protein 1 (OSBP1, also known as OSBP), ceramide-binding protein and four-phosphate adaptor protein 1 and 2.

In this study, we employed targeted RNA interference in combination with lipid mass spectrometry, and chemical interference to identify host factors controlling processes in lipid metabolism for rhinovirus infection. Our data support a PI4P-cholesterol counter-current model at ER-Golgi contact sites (Mesmin et al., 2013). We extend this model by showing that HRV-A1A and A16 infections require PI-transfer protein beta (PITPb). PITPb transfers PI and phosphatidylcholine (PC) between membranes *in vitro*, localizes to the Golgi and is required for retrograde transport (Carvou et al., 2010). We also demonstrate that HRV-A16 is dependent on the cholesteryl-esterase hormone-sensitive-lipase (HSL), whereas HRV-A1A is more dependent on endosome and Golgi-associated OSBP-like (OSBPL) proteins, such as OSBPL1, L5, L9, L11, and the lipid droplet (LD) associated OSBPL2. OSBP1 and OSBPL proteins form a large, evolutionarily conserved family of lipid-binding proteins that mediate sterol signalling and transport between membrane compartments, and hence contribute to membrane dynamics and lipid flow. Our data provide a paradigm for ER-Golgi membrane flux in the absence of a functional secretory pathway in rhinovirus infected cells.

Results

The lipid kinase PI4K3b is required for HRV replication

HRV serotypes from species A and B require PI4Ks for infection, as suggested by studies with chemical inhibitors (Spickler et al., 2013; van der Schaar et al., 2013). To determine which PI4Ks were required for HRV infection and replication, we used a pool of small interfering RNAs (siRNA) directed against the known PI4Ks. We addressed PI4K2a (PI4K class 2 alpha), 2b, 3a and 3b, and tested effects on replication of five HRVs encompassing HRV-A species (HRV-A1A, HRV-A2, HRV-A16) and B species (HRV-B14, HRV-B37). HRV-A16, B14 and B37 are ICAM-tropic major rhinoviruses, whereas HRV-A1A and A2 are LDLR-tropic minor rhinoviruses. In addition, we used the enterovirus Coxsackievirus B3 (CVB3) which requires PI4K3b for replication (Hsu et al., 2010). The knock-down of PI4K3b inhibited the infection with all tested HRV-types and also CVB3 in the range of 31% to 80% as scored by immunofluorescence high-throughput assay using a double-stranded (ds) RNA antibody (Fig. 1A, and Suppl. Fig. S1A, Jurgeit et al., 2012; Jurgeit et al., 2010). This was confirmed by Western blotting of cell extracts with an antibody against PI4K3b, and cytotoxicity assessments by cell number measurements (Fig. 1B). The knock-down of PI4K2a inhibited infection of all HRV-types tested, particularly strongly the minor HRV-A1A and A2, but not CVB3, possibly highlighting a common endocytic or replication requirement for HRVs. PI4K3a knock-down strongly inhibited infection with minor HRV-A1A and A2 and also reduced the cell numbers, although this was independent of infection inhibition, suggesting that minor HRV infections require a functional secretory pathway. Although PI4K3a knock-down inhibited infection with minor HRV-A1A and A2, inhibitors of PI4K3a activity, such as AL-9 did not affect HRV replication (data not shown, Bianco et al., 2012). PI4K2b knock-down inhibited HRV-A2 but not other rhinoviruses or CVB3 (Suppl. Fig. 1A,B).

Prior genome-wide RNA interference screens suggested that PI4K3b was involved in HRV-A1A and A16 infection (Greber lab, unpublished results). To further explore a role of PI4K3b in HRV infection, we employed the synthetic PI4K3b inhibitor PIK93. PIK93 inhibits PI4K3b activity with *in vitro* half inhibitory concentration (IC_{50}) of 19 nM, and PI4K3a with IC_{50} of 1 µM (Knight et al., 2006). In both HeLa and primary human airway epithelial cells of nasal biopsies (hAECN), PIK93 blocked infection with all HRV types tested (A1A, A2, B14, A16, B37) and CVB3 with effective concentrations (EC_{50}) ranging from 170 nM to 915 nM for HRV-A2 and HRV-A1A, respectively (Fig. 1C, and Suppl. Fig.

1C-E). Importantly, PIK93 had minimal effects on metabolic activity (Suppl. Fig. 1F). The PIK93 inhibitory profiles against HRVs corresponded well with the anti-viral efficacy of PI4K3b siRNAs, and surprisingly showed little effects on HRV-A1A (Fig. 1A). Further tests using rt-PCR for viral RNA measurements, entry bypass assays using genomic RNA transfections and time controlled drug additions to cells showed that PIK93 blocked viral replication rather than entry (Suppl. Fig. 1G-L). Interestingly, HRV-A1A infection was less sensitive to PIK93 than transfection of viral RNA, suggesting that steps in entry render HRV-A1A relatively insensitive to PIK93, compared to HRV-A16. The specific PI4K3b inhibitor GSK2998533A blocked HRV and CVB3 infections of HeLa cells with EC_{50} values of about 30-100 nM confirming the role of PI4K3b for HRV infection (Suppl. Fig. 1 M,L). As expected, all HRVs and CVB3 were strongly inhibited by the fungal metabolite Brefeldin A (BFA, 10 μM, Fig. 1C).

Cytoplasmic PI4P levels are increased near HRV replication sites

We used ion chromatography with suppressed conductivity detection to determine the levels of PI4P in HRV-A1A and A16 infected HeLa cells 30 min or 7 h pi. To account for variability in lipid extraction, we normalized the results to the mass of cardiolipin (CL). PIK93 slightly reduced the PI4P levels compared to uninfected control cells indicating that PI4K3b contributes to maintain the levels of PI4P at steady state (Fig. 2A). At 30 min pi, infected cells had reduced levels of PI4P compared to uninfected cells. This decrease correlated with an increase of the $PI4,5P_2$ levels by about 20% independent of PIK93 treatment (data not shown). This suggests that PI4P is converted to $PI4,5P_2$ during HRV entry independent of PI4K3b activity. At 7 h pi, the PI4P level increased by about 30% in HRV-A1A or A16 infected cells compared to uninfected cells. This increase in PI4P lipids was not due to enhanced levels of PI4K3b as shown by Western blotting (Fig. 2B). It was, however, blunted by PIK93 but without affecting the levels of PI4K3b in HRV-A16 infected cells. The data demonstrate that PI4P lipids are increased at the time of HRV RNA replication owing to PI4K3b activity.

We next investigated the subcellular location of PI4P in digitonin-permeabilised cells using an immunofluorescence-based assay specifically detecting cytoplasmic PI4P. Compared to uninfected cells, the cytoplasmic PI4P signals increased in HRV-A1A or A16 infected cells, predominantly in the vicinity of newly synthesized VP2 around the

nucleus, for example 8 h but not 1 h pi (Fig. 2C,D). We also found that PI4K3b localized in the proximity of replicated viral RNA by immune-staining PI4K3b and dsRNA (Fig. 2E). Interestingly, a small amount of dsRNA-positive foci dispersed from the bulk were found to be PI4K3b negative. In uninfected cells, PI4K3b colocalized with the peripheral cytoplasmic TGN marker p230 and the cis-Golgi marker GM130 but not the ER marker calnexin (Fig. 2F). In infected cells, newly synthesized VP2 colocalized with p230, GM130 and the ER-Golgi intermediate compartment marker ERGIC53 in perinuclear clusters of punctate fluorescence (Suppl. Fig. 2A-C). Intriguingly, the perinuclear VP2-positive areas appeared to be enriched in calnexin, suggesting that HRV infection reorganized cellular compartments (Suppl. Fig. 2D).

To test a functional involvement of the TGN, we subjected the cells to Exo2, a small compound disrupting the TGN and early endosomes but not the ER or ERGIC (see Suppl. Fig. 2E, and Spooner et al., 2008). Exo2 is more specific than BFA which disrupts the TGN and also the cis-Golgi (Suppl. Fig. 2E). Exo2 blocked HRV-A1A and A16 replication in a dose-dependent manner with EC_{50} between 16.2 and 24.6 μM, if added prior to 3 h pi, suggesting an involvement of the TGN in HRV replication (Suppl. Fig. 2F). Together, the data show that PI4P lipids are produced by PI4K3b in the vicinity of HRV replication sites near Golgi and ER compartments, and viral replication requires the TGN.

HRV infected cells increase cholesterol and reduce cholesteryl-esters

Cells infected with enteroviruses, including rhinoviruses display high levels of positively curved cytoplasmic membranes, as indicated by thin section electron microscopy (see Fig. 3A). But how these membranes receive their lipids has been incompletely explored. Towards elucidating if cholesterol was involved in HRV replication, we analysed the levels of cholesterol by fluorescence microscopy and mass spectrometry. Cholesterol staining with filipin revealed a striking colocalization with VP2 in perinuclear clusters of HRV-A1A or A16 infected cells 8 h pi (Fig. 3B). Fluorescence quantification showed a significant increase in the perinuclear filipin signal 14 h pi, and a trend to increase 8 pi, albeit less pronounced in HRV-A1A than HRV-A16 infected cells (Fig. 3C). These results were confirmed by mass spectrometry in cell populations, showing that population levels of cholesterol increased from 140 μg/ml before infection to 190-220 μg/ml at 7, 15 or 22 h pi with HRV-A16, although not significantly with HRV-A1A compared to uninfected cells

(Fig. 3D, Suppl. Fig. 3A). Concomitantly, the levels of cholesteryl-esters were found to be reduced from 60 or 85 μg/ml before infection to 33 or 56 μg/ml 15 or 22 h pi in HRV-A1A or HRV-A16 infected cells, respectively. This suggests that cholesteryl-esters contribute to increase cholesterol pools in rhinovirus infected cells, although they may not be sufficient to cover the entire surge in cholesterol in HRV-A16 infected cells.

Distinct mechanisms can increase the levels of cholesterol in the ER membrane. One is *de novo* biosynthesis from acetyl CoA through the mevalonate pathway on ER membranes including the rate limiting enzyme HMG-CoA reductase. A second one is uptake of extracellular cholesterol via late endosomes, or third, hydrolysis of cholesteryl-esters in LDs or late endosomes (Ikonen, 2008). To determine whether *de novo* biosynthesis was required for HRV replication, we tested the effect of small chemical inhibitors of cholesterol metabolism on HRV infection and replication (Fig. 3E). HeLa cells were infected with HRV-A1A or A16 at MOI 20, treated with compounds and stained by anti-VP2 antibodies 8, 10, 12 or 14 h pi, or were analysed for replication of viral RNA by quantitative rt-PCR. 25-HC is produced from cholesterol by cholesterol 25-hydroxylase (CH25H) and inhibits one of the rate limiting enzymes in cholesterol biosynthesis 3-hydroxy-3-methylglutaryl-coenzyme A (HMG-CoA) reductase (Kandutsch and Chen, 1974), and also blocks OSBP1 (Mesmin et al., 2013; Wang et al., 2008). 25-HC strongly inhibited HRV-A1A and HRV-A16 infection and replication, comparable to PIK93 (Fig. 3F,G, and Fig. 1E,F). 25-HC also inhibited the expression of HMG-CoA reductase mRNA in uninfected cells to levels similar as in infected cells not treated with compound (Fig. 3H). In addition, 25-HC and methyl-β-cyclodextrin (MβCD), which depletes cells of cholesterol by extracting free cholesterol from membranes, inhibited HRV-A1A or A16 infections under conditions, where the inoculum was washed off the cells 1 h pi, compounds added 2 h pi and infection scored 8 or 14 h pi (Suppl. Fig. 3B). These results were similar to PIK93, and highlight that cholesterol is required for one or several post entry steps in HRV infection and replication. In contrast, compactin or AY9944, which inhibit cholesterol biosynthesis at early or late steps by blocking HMG-CoA reductase, or Δ^7-dehydrocholesterol reductase, respectively, had relatively little effect, since the drug treatments led to 10-30% reduction in HRV-A16 and 50% reduction in HRV-A1A infection at 8 h pi, but no effects were visible anymore at 10, 12 or 14 h pi (Fig. 3F-H). Neither MβCD, AY9944 nor compactin showed adverse toxicity in the resazurin metabolic assay (Suppl. Fig. 3C). As expected, the cholesterol biosynthesis inhibitors compactin (10 μM) or AY9944 (10 μM) did not reduce but rather increased the expression of HMG-CoA

reductase. Likewise, these compounds did not inhibit HRV infection of hAECN, as measured by dsRNA immunofluorescence (data not shown). The data suggest that cholesterol biosynthesis has little role in HRV replication, although cholesterol crucially supports replication.

HRV infections cluster lipid droplets near replication centers and require hormone sensitive lipase

To further explore the mechanism of cholesterol increase in rhinovirus infected cells, we investigated if LDs were involved in infection. LDs contain neutral lipids such as cholesteryl-esters or triacylglycerol and a monolayer of phospholipids, as well as a key set of proteins (Walther and Farese, 2012). Compared to uninfected cells, the size and shape of LDs stained with LD540 and scored by fluorescence microscopy did not significantly change in infected cells 8 h pi (Fig. 4A,B). At 14 h pi, however, fewer and bigger LDs were detected, and some of them colocalized with puncta of newly synthesized VP2.

We determined if hydrolysis of cholesteryl-esters was implicated in HRV infection by treating cells with an inhibitor of HSL which catalyzes the hydrolysis of cholesteryl-esters, tri-, di-, and monoacyl-glycerols and is associated with LDs. The pretreatment of cells with the HSL inhibitor CAY10499 reduced HRV-A1A and A16 infections in a dose-dependent manner with EC_{50} of 0.35 and 5.2 μM at 8 h pi (Fig. 4C). Addition of CAY10499 to cells after infection decreased HRV inhibition less effectively (EC_{50} values between 4 to 92.9 μM) depending on the HRV type and the time of addition (Fig. 4D). This was in accordance with the report that the inhibition of HSL cholesteryl-esterase activity with CAY10499 required prolonged inhibitor pretreatment (Manna et al., 2013). Importantly, CAY10499 was not toxic up to 64 μM (Fig. 4E). In addition, RNA interference against HSL significantly inhibited replication of HRV-A16 but not HRV-A1A (Fig. 4F-H). The data show that some rhinoviruses take advantage of host lipases to produce cholesterol from cholesteryl-esters, and thereby enhance replication on Golgi-derived membranes.

To address how HRV-A1A accesses cholesterol, we conducted an siRNA miniscreen against OSBP-like proteins (OSBPL), also called OSBP-related proteins (ORPs). OSBPL

are intracellular sterol sensors or transporters, frequently located at membrane contact sites (Olkkonen and Li, 2013). Strikingly, HRV-A1A was inhibited by RNAi against OSBPL1, L2, L5, L6, L7, L8, L9, L10 and L11, but not L3 or L4, while the other rhinoviruses and CVB3 were less dependent on OSBPLs (Fig. 4H, Suppl. Fig. 4A-D). OSBPL1, L2 and L5 are implicated in ER-late endosomes or ER-LDs contacts, and L3 and L4 in ER-plasma membrane contact sites (Olkkonen and Li, 2013). Notably, OSBPL2 is associated with LDs, and its knock-down increases cholesteryl-ester synthesis (Hynynen et al., 2009), and thereby could inhibit HRV-A1A infection. OSBPL5, which is located on the ER has been implicated in cholesterol exit from late endosomes and lysosomes (Du et al., 2011). Interestingly, OSBPL9 and L11 were involved not just in HRV-A1A but also A2, B14 and A16 but not B37 or CVB3 infections, and localized near HRV-A1A or A16 replication sites (Suppl. Fig. 4A). OSBPL11 pairs with OSBPL9 and localizes at the Golgi-endosome interface (Olkkonen and Li, 2013). Together the data suggest that late endosomes can supply cholesterol for rhinovirus replication. For HRV-A1A, an involvement of late endosomes may compensate for LD-associated cholesteryl-ester hydrolysis.

The PI4P-cholesterol exchange protein OSBP1, VAP-B, Sac1 and PITPb are required for HRV replication

Several lines of evidence pointed to an involvement of the PI4P-cholesterol exchange protein OSBP1 in HRV infection, namely the increase in both PI4P and cholesterol levels at stages of viral replication, the sensitivity of HRV infection to 25-HC and infection independence of cholesterol biosynthesis. The latter supported the notion that 25-HC inhibited HRV infection by blocking OSBP1. In accordance with this, the treatment of cells with 25-HC induced the clustering of OSBP1 in perinuclear Golgi-like areas (Suppl. Fig. 5A). This was consistent with the finding that 25-HC not only blocks the ability of OSBP1 to extract sterols from the ER through its lipid transport domain (ORD), but also extraction of PI4P from the Golgi, and hence leads to accumulation of OSBP1 at Golgi-ER interface (Mesmin et al., 2013; Wang et al., 2008).

We determined the EC_{50} for 25-HC mediated enterovirus infection inhibition in HeLa and primary cells for HRV-A1A, A2, B14, A16, B37 and CVB3. For HRV-A types, 25-HC EC_{50} were below 1 µM, for the B-types close to 1 µM, and for CVB3 about 4 µM without

metabolic toxicity (Fig. 5A-C, and Suppl. Fig. 5A-E). In hAECN cells, the EC_{50} values for 25-HC were around 1 μM for the HRV-A types and around 2 μM for the HRV-B types (Fig. 5C, and Suppl. Fig. 5D). 25-HC did not inhibit CVB3 replication in hAECN cells up to 10 μM, and did not affect the metabolic activity of cells up to 10 μM during 8 or 24 h periods of incubation (Fig. 5B). Time course addition experiments showed that 25-HC addition at 1 or 3 h pi was nearly as effective at inhibiting HRV-A, HRV-B or CVB3 as when added prior to infection, although the EC_{50} were slightly higher upon addition pi (Fig. 5D, and Suppl. Fig. 5F). This shows that 25-HC has minor effects on steps prior to replication. When added 5 h pi at the onset of replication, however, 25-HC did not inhibit infections, indicating that it blocked initiation of the viral replication membranes.

To further test if OSBP1 is specifically required for HRV replication, we knocked-down OSBP1 by RNA interference. OSBP1 knock-down was very efficient, and inhibited infection with all HRV types tested and CVB3, although the effects on HRV-B14, B37 and CVB3 were not as pronounced as on HRV-A1A, A2 and A16 (Fig. 5E,F). This provides strong evidence that OSBP1 broadly enhances enterovirus infection. OSBP1 is an 807-amino acid multi-domain protein with an N-terminal PH domain, an FFAT (two phenylalanines in an acidic track) motif and a C-terminal ORD domain (Fig. 5G). It localizes at ER-Golgi contact sites by binding simultaneously Golgi PI4P through its PH domain, and the ER vesicle-associated membrane protein (VAMP)-associated protein A or B (VAP-A, B) via its FFAT motif. Expression of FLAG (phenylalanine-leucine-alanine-glycine)-tagged OSBP1 in uninfected cells showed a tight localization of the protein in a perinuclear area, reminiscent of Golgi localization (Fig. 5H, and Amako et al., 2009). In HRV-A1A or A16 infected cells, FLAG-OSBP1 was more dispersed than in uninfected cells, and localized to areas positive for VP2, for example 8 h pi. An OSBP mutant lacking the PH domain (ΔPH-OSBP1) was distributed throughout the cytoplasm, but not on the Golgi. Its expression led to a clear reduction of VP2 signals suggesting that it reduced infection by acting as a dominant-negative protein interfering with the function of the endogenous OSBP1, possibly displacing endogenous OSBP1 from VAP-B. Strikingly, ΔPH-OSBP1 did not colocalize with VP2, indicating that the PH domain binding to PI4P was crucial for the recruitment of OSBP1 to newly synthesized viral protein.

OSBP1 and also yeast Osh4p shuttle cholesterol against a concentration gradient of cholesterol from the ER to the Golgi, and this involves the ER-associated OSBP1 binding protein vesicle-associated membrane protein-associated protein (VAP) A, the ER-

associated PI4P phosphatase Sac1 and the PI-transfer protein PITPb (de Saint-Jean et al., 2011; Mesmin et al., 2013; Olkkonen and Li, 2013). The driving force for cholesterol shuttling against its concentration gradient comes from shuttling PI4P along its concentration gradient from Golgi to ER, at ER-Golgi contact sites. Using RNA interference, we found that the knock-down of VAP-B, Sac1 or PITPb inhibited infection with HRV-A1A and A16, as measured by dsRNA high-throughput fluorescence microscopy or Western blotting with an antibody against VP2, which also detects the viral polyprotein precursor VP0 (Fig. 5I,J). The data support a model where a cycle of PI4P, cholesterol and PI lipids between the ER and the Golgi drives the replication of rhinovirus on Golgi membranes in close proximity to the ER.

Discussion

How different lipid species act together to build up viral replication compartments is poorly understood. We analysed host factors controlling the flux of the phosphoinositide PI4P, and the neutral lipids cholesterol and cholesteryl-esters in rhinovirus infected cells (Fig. 6A). Increased levels of PI4P were found on Golgi membranes of infected cells by virtue of PI4K3b, and cholesterol was increased near viral replication sites. The lipid transfer protein OSBP1 exchanges PI4P with cholesterol at membrane contact sites, and is broadly required for rhinovirus replication, as well as the ER phosphatase Sac1 hydrolyzing PI4P, presumably to preclude PI4P competition for sterol binding on OSBP1.

We also show that rhinovirus infected cells utilize cholesteryl-esters from LDs or late endosomes to produce cholesterol, which is key for replication. Our model depicted in Fig. 6B extends a recently proposed one-to-one counter-current sterol to PI4P gradient model for forward trafficking of sterols from the ER to the Golgi (de Saint-Jean et al., 2011; Mesmin et al., 2013). Lipid flux between adjacent membrane compartments may be akin to treadmilling of polymer subunits in cytoskeletal filaments. Yet, the PI4P-cholesterol flux likely involves the coupling of additional lipids in rhinovirus replication, such as PC through PITPb. This may enhance the complexity of lipids building up the membranous web for the replication of positive-sense RNA viruses. These lipids likely co-determine membrane curvature, dynamics, recruitment of effector proteins, including viral polymerase, or may simply counteract the loss of secretory membrane flux imposed by viral proteins.

Rhinovirus replication is initiated on Golgi membranes

We show that a range of rhinoviruses require Golgi membranes and PI4K3b to establish their replication sites in the proximity of the TGN, the ER and ERGIC, in line with other enteroviruses, such as poliovirus, CVB3, enterovirus 71 (Belov and van Kuppeveld, 2012; Hsu et al., 2010; Spickler et al., 2013). HRV replication critically depended on the activity of PI4K3b. PI4K3b was not increased during HRV replication, but recruited to sites of RNA replication where it increased the pool of PI4P lipids. Both HRV-A1A and A16 upregulated PI4P lipids, and this was blunted by the PI4K3b inhibitor PIK93, which is known to block replication of HRV-A, B and C types (Mello et al., 2014; Spickler et al., 2013). The data also provide validation for an emerging anti-viral concept, namely to blunt virus-induced cellular activities by inhibiting but not eliminating host factors, and thereby gaining anti-viral efficacy with minimal collateral damage.

We also found that rhinovirus infection depended on PI4K2a, which localizes to the TGN and endosomes and participates in vesicular trafficking between endosomes and TGN (Wang et al., 2003). Using population measurements in presence of PIK93, PI4K2a activity was apparently not increased in infection, raising the possibility that PI4K2a controls a constitutive process, possibly virus uptake into cells, and may not globally induce PI4P levels to support infection. This does not exclude a local induction of PI4K2a activity, for example similar to the entry of adenovirus, which activates about 3% of the total cellular pool of protein kinase A (Suomalainen et al., 2001). Interestingly, PI4K3a, which controls the formation of ER exit sites (Farhan et al., 2008), supported infection with the minor HRV-A1A and A2 types, and could be involved in the entry or replication of LDL-receptor tropic HRVs.

Cholesterol and cholesteryl-esters are crucial for HRV replication

Rhinovirus infected cells have high levels of positively curved cytoplasmic membranes, similar to other enteroviruses. Cholesterol insertion into a lipid bilayer determines the equilibrium curvature and increases bending stiffness of membranes (Bruckner et al., 2009). One possibility for acquiring cholesterol is receptor-mediated endocytosis, as suggested for poliovirus and coxsackievirus (Ilnytska et al., 2013). HRV replication was

not inhibited by the knock-down of Rab5, Rab11, DAB2, HIP1 or Epsin15L, but Rab18 knock-down, which affects the formation of lipid droplets, reduced HRV infection (data not shown). We observed increased levels of cholesterol at sites of replication, although HRV-A1A did not increase the overall cholesterol levels in cells, unlike HRV-A16.

A major fraction of cholesterol increase correlated with a reduction of cholesteryl-esters for both HRV-A1A and A16, and was at least in part due to the cholesteryl-esterase HSL. Notably, mass balance considerations indicated that the decrease in cholesteryl-esters unlikely accounts for the full increase in cholesterol in HRV-A16 infected cells. Interestingly, HSL is associated with LDs particularly upon activation of lipolysis, and hydrolyzes a broad range of cholesteryl esters, trylglycerides, and lipoidal esters (Hashimoto et al., 2012), which could be used to synthesize cholesterol as long as HMG-CoA reductase is available in cells. In fact, we found that LDs coalesced near the rhinovirus replication sites indicating their mobilization. Interestingly, HRV-A1A infection, which occurs through late endosomes was weakly inhibited by CAY10499 (EC_{50} 5.2 μM versus 0.35 μM for HRV-A16), and was not sensitive to knock-down of HSL, raising the possibility that cholesteryl-esters from other organelles than LDs are recruited for HRV-A1A replication. Strikingly, OSBPL1 (also known as ORP1L) and OSBPL5 were required for infection with LDL-receptor dependent HRV-A1A and A2, suggesting a role of late endosomal cholesterol for minor HRVs. OSBPL1 can simultaneously bind Rab7 and VAP on late endosomes and the ER, respectively, and thereby contribute to the formation of membrane contact sites (Rocha et al., 2009). It may assist the recruitment of cholesterol from late endosomes. In addition, OSBPL11 knockdown strongly inhibited HRV but not CV replication. OSBPL11 contains a PH domain that binds to PI4P, and can dimerize with OSBPL9, which is located at ER and Golgi membranes. We speculate that HRV recruits additional cholesterol via OSBPL11 independent of OSBP1.

OSBP1 is a key effector of PI4P and cholesterol flux and drives rhinovirus replication

OSBP1 plays a central role in enterovirus infection. It is found at membrane contact sites, in particular between the ER and Golgi where it binds PI4P and Arf1-GTP through a PH domain, and VAP through its FFAT domain, and thereby functions as a non-vesicular cholesterol transporter equilibrating free cholesterol and PI4P between the ER and the

Golgi (Goto et al., 2012; Mesmin et al., 2013). A PH domain deleted OSBP1 mutant was not found near viral replication sites, but inhibited rhinovirus infection highlighting the importance of OSBP1 binding to PI4P. In addition, OSBP1 integrates cholesterol levels with cell growth (Raychaudhuri and Prinz, 2010). Under conditions of abundant cholesterol, it sequesters protein phosphatases and thereby de-represses MAP kinase signalling and cell growth, or it functions as a sterol-dependent transducer in cytokine signalling through signal transducer and activator of transcription-3 (STAT3) and Janus-activated kinase-2 (JAK2), which phosphorylates OSBP1 and renders it a scaffold for binding STAT3 (Romeo and Kazlauskas, 2008). The engagement of OSBP1 at cholesterol-rich replication sites could thus tune the cytokine response to rhinovirus infection.

Interestingly, OSBP1 is a target of natural and synthetic compounds with therapeutic potential (Burgett et al., 2011). The oxysterol variant 25-HC binds with higher affinity to OSBP1 than cholesterol, locks OSBP1 in a lipid exchange-inactive state, and inhibits replication of rhinoviruses, and also CVB3. This was similar to a report for poliovirus (Arita et al., 2013). Interestingly, 25-HC activates interferon response and has innate antiviral effects (Blanc et al., 2013; Liu et al., 2013). This likely involves an ER docking site for OSBP1, VAP, which is targeted by interferon inducible transmembrane protein 3 (IFITM3), leading to endosomal cholesterol accumulation and inhibition of enveloped virus entry (Amini-Bavil-Olyaee et al., 2013). Interestingly, we observed inhibition of HRV-A16 but not A1A entry with 25-HC (Suppl. Fig. 5E), albeit at higher doses than blocking replication. Collectively, we conclude that rhinoviruses build up PI4P-rich Golgi membranes through PI4K3b to trigger lipid flux. We expect that other viruses than enteroviruses replicating on cytoplasmic membranes upregulate lipid signalling branches to generate membrane asymmetry that is critical for driving lipid counter-flux on replication membranes and thereby enhance viral replication.

Experimental procedures

Chemicals, plasmids and antibodies, cell lines, Western blotting, reverse transcription PCR, image acquisitions and analyses are described in Supplemental Information. Infections were at MOI 20, unless indicated otherwise. Figures were assembled using

Adobe Photoshop and Illustrator. Graphs represent mean values of analysed samples (n) including the SD and p-values from t-tests.

Primary cells and viruses

Human airway epithelial cells from nasal biopsies (hAECN) were cultured as recommended by the supplier (Epithelix, Geneva, Switzerland). HRV-A1A HRV-A2, B14, A16, B37 and CVB3 were used as described (Jurgeit et al., 2010).

Lipid extraction and analyses

Phosphoinositides from HeLa cells were analyzed by ion chromatography with suppressed conductivity detection. Lipids were extracted into chloroform, dried and fractionated by anion-exchange HPLC, and PI4P lipids expressed as normalized to mitochondrial cardiolipin. For cholesterol and cholesteryl-ester analyses, HeLa-O cells were treated with inhibitors, infected with purified HRVs (MOI 50) in DMEM supplemented with 2% FBS and 1% NEA at 37°C. Lipds were extracted into chloroform:methanol and analysed in an Agilent HPLC 1100 system (Agilent) coupled with an Applied AB Sciex 3200 QTrap mass spectrometer (AB Sciex, Foster City, CA). Cholesterol and cholesteryl-esters were separated by an Agilent Zorbax Eclipse XDB-C18 column, and their respective levels normalized to phospholipid levels.

Interference and high-throughput infection

siRNAs (20 nM) were reverse transfected to HeLa-O cells in 96-well plates using serum-free Opti-MEM (Invitrogen) and Lipofectamine RNAiMAX (Invitrogen) according to the manufacturer's protocol for 72 h, and infected with HRVs or CV at MOI 20 for 8 h. Alternatively, cells were treated with chemical compounds, infected with HRV or CV and scored for infection by immunostaining with mabJ2 or anti-VP2 antibodies. Images were acquired with an ImageXpress Micro microscope (Molecular Devices) in automated mode, using a CoolSNAP HQ 12bit gray scale camera (Roper Scientific) and 10x/NA 0.5 objective (Nikon), and analyzed with a custom written script in Matlab (MathWorks, Inc.

Natick, MA, USA). Infection indexes (fraction of infected cells per total cell number) were plotted with GraphPad Prism software (GraphPad) as relative units. Typically, infections under normal conditions yielded 30-40% infected cells.

Immunofluorescence and confocal microscopy

HeLa-O cells on coverslips were treated 1 h prior to infection with compounds or transfected with plasmid DNA using Lipofectamine 200 (Invitrogen) 24 h prior to infection. Plasma membrane and cytoplasmic PI4P pools or other antigens were detected in cells fixed with 4% PFA and permeabilized with 0.2% Triton X-100, blocked for 1 h in PBS supplemented with 1% bovine serum albumin (BSA), followed by primary IgM antibodies in blocking buffer overnight at 4°C followed by Alexa Fluor-488 or -594 secondary antibodies for 1 h. Cholesterol was stained with filipin in PBS for 30 min in cells fixed with 4% PFA. Coverslips were mounted in mounting medium (Dako) and analyzed with an inverted Leica TCS SP5 scanning laser confocal microscope with an HCX PL APO 63×/1.4 oil immersion objective. Images were acquired using LAS AF software (Leica) and processed with ImageJ (National Institutes of Health).

Electron microscopy (EM)

Transmission EM of HeLa cells infected with HRV-A16 (MOI 1) for 15 h at 33°C was carried out as described earlier (Strunze et al., 2011).

Authors contribution

Conceived, performed or interpreted experiments (PSR, ML, FT, LBT, FvK, MRW, UFG), wrote manuscript (PSR, UFG), conceived and coordinated study (UFG).

Acknowledgements

We thank Karin Boucke (University of Zurich, Switzerland) for providing the electron micrographs in Figure 3A, Dr. Raul Andino (University of San Francisco, USA) for sharing unpublished results, Dr. Shihyun You (GlaxoSmithKline, Infectious Disease R&D, North Carolina, USA) for gift of GSK2998533A, Dr. Neil Ridgway (Dalhousie University, Canada), Dr. Vesa Olkkonen (Minerva Foundation Institute for Medical Research, Helsinki, Finland), Dr. Shane Minogue (University College London, UK), Dr. Shamshad Cockcroft (University College London, UK) for antibodies, Dr. Raffaele De Francesco (Istituto Nazionale di Genetica Molecolare, Milano, Italy) for AL-9 compound, and Dr.'s Maarit Suomalainen and Robin Klemm (University of Zurich, Switzerland) for discussions or comments to the text.

Funding

Funding was obtained from the Swiss National Science Foundation (31003A_125477 and 31003A_141222/1 to UFG) and the Research and Technology Development project LipidX from SystemsX.ch (LipidX-2008/011 to UFG and MRW).

References

Amako, Y., Sarkeshik, A., Hotta, H., Yates, J., 3rd, and Siddiqui, A. (2009). Role of oxysterol binding protein in hepatitis C virus infection. J Virol *83*, 9237-9246.

Amini-Bavil-Olyaee, S., Choi, Y.J., Lee, J.H., Shi, M., Huang, I.C., Farzan, M., and Jung, J.U. (2013). The antiviral effector IFITM3 disrupts intracellular cholesterol homeostasis to block viral entry. Cell Host Microbe *13*, 452-464.

Arita, M., Kojima, H., Nagano, T., Okabe, T., Wakita, T., and Shimizu, H. (2013). Oxysterol-binding protein family I is the target of minor enviroxime-like compounds. J Virol *87*, 4252-4260.

Balla, T. (2013). Phosphoinositides: tiny lipids with giant impact on cell regulation. Physiol Rev *93*, 1019-1137.

Belov, G.A., and van Kuppeveld, F.J. (2012). (+)RNA viruses rewire cellular pathways to build replication organelles. Current opinion in virology *2*, 740-747.

Bianco, A., Reghellin, V., Donnici, L., Fenu, S., Alvarez, R., Baruffa, C., Peri, F., Pagani, M., Abrignani, S., Neddermann, P*., et al.* (2012). Metabolism of phosphatidylinositol 4-kinase IIIalpha-dependent PI4P Is subverted by HCV and is targeted by a 4-anilino quinazoline with antiviral activity. PLoS Pathog *8*, e1002576.

Blanc, M., Hsieh, W.Y., Robertson, K.A., Kropp, K.A., Forster, T., Shui, G., Lacaze, P., Watterson, S., Griffiths, S.J., Spann, N.J*., et al.* (2013). The transcription factor STAT-1 couples macrophage synthesis of 25-hydroxycholesterol to the interferon antiviral response. Immunity *38*, 106-118.

Bruckner, R.J., Mansy, S.S., Ricardo, A., Mahadevan, L., and Szostak, J.W. (2009). Flip-flop-induced relaxation of bending energy: implications for membrane remodeling. Biophys J *97*, 3113-3122.

Burgett, A.W., Poulsen, T.B., Wangkanont, K., Anderson, D.R., Kikuchi, C., Shimada, K., Okubo, S., Fortner, K.C., Mimaki, Y., Kuroda, M*., et al.* (2011). Natural products reveal cancer cell dependence on oxysterol-binding proteins. Nat Chem Biol *7*, 639-647.

Carvou, N., Holic, R., Li, M., Futter, C., Skippen, A., and Cockcroft, S. (2010). Phosphatidylinositol- and phosphatidylcholine-transfer activity of PITPbeta is essential for COPI-mediated retrograde transport from the Golgi to the endoplasmic reticulum. J Cell Sci *123*, 1262-1273.

de Saint-Jean, M., Delfosse, V., Douguet, D., Chicanne, G., Payrastre, B., Bourguet, W., Antonny, B., and Drin, G. (2011). Osh4p exchanges sterols for phosphatidylinositol 4-phosphate between lipid bilayers. J Cell Biol *195*, 965-978.

Du, X., Kumar, J., Ferguson, C., Schulz, T.A., Ong, Y.S., Hong, W., Prinz, W.A., Parton, R.G., Brown, A.J., and Yang, H. (2011). A role for oxysterol-binding protein-related protein 5 in endosomal cholesterol trafficking. J Cell Biol *192*, 121-135.

Farhan, H., Weiss, M., Tani, K., Kaufman, R.J., and Hauri, H.P. (2008). Adaptation of endoplasmic reticulum exit sites to acute and chronic increases in cargo load. Embo J *27*, 2043-2054.

Gern, J.E. (2010). The ABCs of rhinoviruses, wheezing, and asthma. J Virol *84*, 7418-7426.

Godi, A., Pertile, P., Meyers, R., Marra, P., Di Tullio, G., Iurisci, C., Luini, A., Corda, D., and De Matteis, M.A. (1999). ARF mediates recruitment of PtdIns-4-OH kinase-beta and stimulates synthesis of PtdIns(4,5)P2 on the Golgi complex. Nat Cell Biol *1*, 280-287.

Goto, A., Liu, X., Robinson, C.A., and Ridgway, N.D. (2012). Multisite phosphorylation of oxysterol-binding protein regulates sterol binding and activation of sphingomyelin synthesis. Mol Biol Cell *23*, 3624-3635.

Hashimoto, T., Segawa, H., Okuno, M., Kano, H., Hamaguchi, H.O., Haraguchi, T., Hiraoka, Y., Hasui, S., Yamaguchi, T., Hirose, F.*, et al.* (2012). Active involvement of micro-lipid droplets and lipid-droplet-associated proteins in hormone-stimulated lipolysis in adipocytes. J Cell Sci *125*, 6127-6136.

Heaton, N.S., and Randall, G. (2011). Multifaceted roles for lipids in viral infection. Trends Microbiol *19*, 368-375.

Hsu, N.Y., Ilnytska, O., Belov, G., Santiana, M., Chen, Y.H., Takvorian, P.M., Pau, C., van der Schaar, H., Kaushik-Basu, N., Balla, T.*, et al.* (2010). Viral reorganization of the secretory pathway generates distinct organelles for RNA replication. Cell *141*, 799-811.

Hynynen, R., Suchanek, M., Spandl, J., Back, N., Thiele, C., and Olkkonen, V.M. (2009). OSBP-related protein 2 is a sterol receptor on lipid droplets that regulates the metabolism of neutral lipids. J Lipid Res *50*, 1305-1315.

Ikonen, E. (2008). Cellular cholesterol trafficking and compartmentalization. Nat Rev Mol Cell Biol *9*, 125-138.

Ilnytska, O., Santiana, M., Hsu, N.Y., Du, W.L., Chen, Y.H., Viktorova, E.G., Belov, G., Brinker, A., Storch, J., Moore, C.*, et al.* (2013). Enteroviruses harness the cellular endocytic machinery to remodel the host cell cholesterol landscape for effective viral replication. Cell Host Microbe *14*, 281-293.

Jacobs, S.E., Lamson, D.M., St George, K., and Walsh, T.J. (2013). Human rhinoviruses. Clin Microbiol Rev *26*, 135-162.

Jurgeit, A., McDowell, R., Moese, S., Meldrum, E., Schwendener, R., and Greber, U.F. (2012). Niclosamide is a proton carrier and targets acidic endosomes with broad antiviral effects. PLoS Pathog *8*, e1002976; 1002910.1001371/journal.ppat.1002976.

Jurgeit, A., Moese, S., Roulin, P., Dorsch, A., Lötzerich, M., Lee, W.-M., and Greber, U.F. (2010). An RNA replication-center assay for high content image-based quantifications of human rhinovirus and coxsackievirus infections. Virology journal *7*, 264.

Kandutsch, A.A., and Chen, H.W. (1974). Inhibition of sterol synthesis in cultured mouse cells by cholesterol derivatives oxygenated in the side chain. J Biol Chem *249*, 6057-6061.

Knight, Z.A., Gonzalez, B., Feldman, M.E., Zunder, E.R., Goldenberg, D.D., Williams, O., Loewith, R., Stokoe, D., Balla, A., Toth, B.*, et al.* (2006). A pharmacological map of the PI3-K family defines a role for p110alpha in insulin signaling. Cell *125*, 733-747.

Liu, S.Y., Aliyari, R., Chikere, K., Li, G., Marsden, M.D., Smith, J.K., Pernet, O., Guo, H., Nusbaum, R., Zack, J.A.*, et al.* (2013). Interferon-inducible cholesterol-25-hydroxylase broadly inhibits viral entry by production of 25-hydroxycholesterol. Immunity *38*, 92-105.

Manna, P.R., Cohen-Tannoudji, J., Counis, R., Garner, C.W., Huhtaniemi, I., Kraemer, F.B., and Stocco, D.M. (2013). Mechanisms of action of hormone-sensitive lipase in mouse Leydig cells: its role in the regulation of the steroidogenic acute regulatory protein. J Biol Chem *288*, 8505-8518.

Mello, C., Aguayo, E., Rodriguez, M., Lee, G., Jordan, R., Cihlar, T., and Birkus, G. (2014). Multiple classes of antiviral agents exhibit in vitro activity against human rhinovirus type C. Antimicrob Agents Chemother *58*, 1546-1555.

Mesmin, B., Bigay, J., Moser von Filseck, J., Lacas-Gervais, S., Drin, G., and Antonny, B. (2013). A four-step cycle driven by PI(4)P hydrolysis directs sterol/PI(4)P exchange by the ER-Golgi tether OSBP. Cell *155*, 830-843.

Olkkonen, V.M., and Li, S. (2013). Oxysterol-binding proteins: sterol and phosphoinositide sensors coordinating transport, signaling and metabolism. Progress in lipid research *52*, 529-538.

Raychaudhuri, S., and Prinz, W.A. (2010). The diverse functions of oxysterol-binding proteins. Annu Rev Cell Dev Biol *26*, 157-177.

Reiss, S., Rebhan, I., Backes, P., Romero-Brey, I., Erfle, H., Matula, P., Kaderali, L., Poenisch, M., Blankenburg, H., Hiet, M.S.*, et al.* (2011). Recruitment and activation of a lipid kinase by hepatitis C virus NS5A is essential for integrity of the membranous replication compartment. Cell Host Microbe *9*, 32-45.

Rocha, N., Kuijl, C., van der Kant, R., Janssen, L., Houben, D., Janssen, H., Zwart, W., and Neefjes, J. (2009). Cholesterol sensor ORP1L contacts the ER protein VAP to control Rab7-RILP-p150 Glued and late endosome positioning. J Cell Biol *185*, 1209-1225.

Romeo, G.R., and Kazlauskas, A. (2008). Oxysterol and diabetes activate STAT3 and control endothelial expression of profilin-1 via OSBP1. J Biol Chem *283*, 9595-9605.

Sharp, T.M., and Estes, M.K. (2010). An inside job: subversion of the host secretory pathway by intestinal pathogens. Current opinion in infectious diseases *23*, 464-469.

Spickler, C., Lippens, J., Laberge, M.K., Desmeules, S., Bellavance, E., Garneau, M., Guo, T., Hucke, O., Leyssen, P., Neyts, J.*, et al.* (2013). Phosphatidylinositol 4-kinase III beta is essential for replication of human rhinovirus and its inhibition causes a lethal phenotype in vivo. Antimicrob Agents Chemother *57*, 3358-3368.

Spooner, R.A., Watson, P., Smith, D.C., Boal, F., Amessou, M., Johannes, L., Clarkson, G.J., Lord, J.M., Stephens, D.J., and Roberts, L.M. (2008). The secretion inhibitor Exo2 perturbs trafficking of Shiga toxin between endosomes and the trans-Golgi network. Biochem J *414*, 471-484.

Strunze, S., Engelke, M.F., Wang, I.-H., Puntener, D., Boucke, K., Schleich, S., Way, M., Schoenenberger, P., Burckhardt, C.J., and Greber, U.F. (2011). Kinesin-1-mediated capsid disassembly and disruption of the nuclear pore complex promote virus infection. Cell Host Microbe *10*, 210-223.

Suomalainen, M., and Greber, U.F. (2013). Uncoating of non-enveloped viruses. Current opinion in virology *3*, 27-33.

Suomalainen, M., Nakano, M.Y., Boucke, K., Keller, S., and Greber, U.F. (2001). Adenovirus-activated PKA and p38/MAPK pathways boost microtubule-mediated nuclear targeting of virus. The EMBO journal *20*, 1310-1319.

van der Schaar, H.M., Leyssen, P., Thibaut, H.J., de Palma, A., van der Linden, L., Lanke, K.H., Lacroix, C., Verbeken, E., Conrath, K., Macleod, A.M.*, et al.* (2013). A novel, broad-spectrum inhibitor of enterovirus replication that targets host cell factor phosphatidylinositol 4-kinase IIIbeta. Antimicrob Agents Chemother *57*, 4971-4981.

Walther, T.C., and Farese, R.V., Jr. (2012). Lipid droplets and cellular lipid metabolism. Annu Rev Biochem *81*, 687-714.

Wang, P.Y., Weng, J., Lee, S., and Anderson, R.G. (2008). The N terminus controls sterol binding while the C terminus regulates the scaffolding function of OSBP. J Biol Chem *283*, 8034-8045.

Wang, Y.J., Wang, J., Sun, H.Q., Martinez, M., Sun, Y.X., Macia, E., Kirchhausen, T., Albanesi, J.P., Roth, M.G., and Yin, H.L. (2003). Phosphatidylinositol 4 phosphate regulates targeting of clathrin adaptor AP-1 complexes to the Golgi. Cell *114*, 299-310.

Figure Legends

Figure 1: PI4K3b and PI4K3a support replication of rhinoviruses (refers to Suppl. Fig. S1)

(A) Effects of siRNAs against PI4K2a, PI4K3a or PI4K3b (pool of 4 distinct siRNAs each), or with the negative control siRNA (all star, *) on HRV-A1A, A2, A16, B14, B37 or CVB3 infection. Values represent means ± SD, n=2.

(B) Western blots of lysates from HeLa cell infected with HRV-A16 (MOI 50) probed with antibodies against PI4K2a, PI4K3a, PI4K3b, or glyceraldehyde-phosphate dehydrogenase (GAPDH).

(C) Drug treatments of HeLa (white bars) or hAECN (black bars) 1 h prior to infection, including DMSO, brefeldin A (BFA) and PIK93. EC_{50} values of inhibitors on infections (8 h for HeLa, or 18 h for hAECN) were obtained by nonlinear regression of the data fitted to the variable-slope sigmoidal dose-response. Values represent means ± SD, n=2.

Figure 2: PI4P and PI4K3b are enriched on rhinovirus replication sites (refers to Suppl. Fig. S2)

(A) Total lipids extraction and PI4P measurement by ion chromatography with suppressed conductivity detection from HeLa cells treated with DMSO or 1 μM PIK93 1 h prior to infection with HRV-A1A or HRV-A16 (MOI 50). Values were normalized to cardiolipin (CL) and represent means ± SD, n=3.

(B) No gross reduction of PI4K3b levels detected by Western blotting upon treatment of cells with PIK93 inoculated with HRV-A16 or UV-treated HRV-A16 (MOI 50) for 8 h. Values are means ± SD, n=3.

(C) HeLa cells infected with HRV-A1A or HRV-A16 (MOI 20) for 8 h were stained for viral protein VP2 (green), cytoplasmic PI4P (red), and nuclei with DAPI (blue). Scale bar: 10 μm.

(D) HeLa cells infected with HRV-A1A or HRV-A16 were stained for cytoplasmic PI4P (green) and nuclei (blue). The total intensity of perinuclear PI4P signal for each cell was measured and normalized to the corresponding area. Values are means ± SD, n≥36.

(E,F) HeLa cells infected with HRV-A1A or HRV-A16 (8 h) were stained for dsRNA (green), PI4K3b (red) and DAPI (nuclei, blue). Non-infected cells were stained for p230, GM130 or calnexin (green) and PI4K3b (red). Scale bar: 10 µm.

Figure 3: Cholesterol is enriched on HRV replication sites (refers to Suppl. Fig. S3)

(A) Electron micrographs of HeLa cells infected with HRV-A16 (MOI 1), or uninfected cells, Epon embedded and stained with uranyl acetate. Positively curved viral replication membranes are shown by arrow heads, areas with multiple membranes closely apposed are highlighted by double arrow heads, and lipid droplets indicated by *.

(B) HeLa cells infected with HRV-A1A or HRV-A16 for 8 h were stained for VP2 (green) and cholesterol (blue). Scale bar: 10 µm.

(C) Quantification of filipin signal representing total cholesterol for each cell normalized to its area. Values are means ± SD, n≥7.

(D) Quantification of cholesterol and cholesteryl-esters by mass spectrometry normalized to the phospholipid (PL) in HRV-A1A and HRV-A16 infected cells (MOI 50). Values are means ± SD, n=3.

(E) Depiction of the cholesterol biosynthesis pathway with the limiting-rate HMG-CoA reductase, and inhibitors of early and late cholesterol biosynthesis (compactin and AY9944 respectively), the cholesterol-depleting agent (MβCD) and the OSBP1 ligand 25-HC depicted in red.

(F) Infection profiles of HeLa cells infected with HRV-A1A or HRV-A16 in presence or absence of 25-HC, compactin or AY9944 added 1 h pi. The ratio of infected cells was calculated and normalized to the mock control. Values are means ± SD, n=2.

(G) Viral replication measured by rt-PCR of HRV 5’ UTR in HeLa cells infected with HRV-A1A or HRV-A16 (8 h) and treated with 25-HC, PIK93, compactin or AY9944 1 h prior to

infection. Data are normalized to the respective geometric means of GAPDH, transferrin receptor (TRFC) and eukaryotic elongation factor (EEF).

(H) Reduction of HMG-CoA reductase expression in HRV-A1A or HRV-A16 infected cells measured by rt-PCR normalized to the respective geometric means of GAPDH, TRFC and EEF. Values are means ± SD, n=3.

Figure 4: Lipid droplets are a source of cholesterol source for HRV-A16 replication (refers to Suppl. Fig. S4)

(A) HeLa cells infected with HRV-A1A or HRV-A16 were stained for lipid droplets (LD = green), VP2 (red) and nuclei (DAPI, blue). Scale bar: 10 µm.

(B) CAY10499, an inhibitor of LD associated cholesteryl-esterase inhibits HRV-A16 and to a lesser extent HRV-A1A. Infection was scored by determining the ratio of infected cells normalized to uninfected controls. EC_{50} values were obtained by nonlinear regression of the data fitted to the variable-slope sigmoidal dose-response. Values are means ± SD, n=2.

(C, D) Pre- rather than post entry addition of CAY10499 inhibits infection with HRV-A16 and to a lesser extent HRV-A1A. Infection and EC_{50} values were determined as described in (B). Values are means ± SD, n=2.

(E) CAY10499 does not affect the metabolic activity of cells up to 64 µM compared to DMSO solvent and 0.01% SDS (positive control) upon treatments as determined by resazurin assays. Values are means ± SD, n=4.

(F) Knock-down of HSL with a pool of 4 siRNAs inhibits HRV-A16 but not HRV-A1A infection compared with the negative control siRNA (all star). Values: mean ± SD, n=2.

(G) Western blots against HSL from lysates of HeLa cells infected with HRV-A16 (MOI 50, 8 h), including the viral proteins VP0 and VP2 (mab 16-7, Jurgeit et al., 2010) and GAPDH.

(H) RNA interference against OSBPL proteins differentially affects infection with HRV-A1A, A2, B14, A16, B37 and CVB3 as indicated by dsRNA infection readout in high-

throughput microscopy assays 8 h pi. Minor HRV are denoted by *. Related to Suppl. Fig. 4.

Figure 5: OSBP1 broadly supports enterovirus infections (refers to Suppl. Fig. S5)

(A) 25-HC blocks HRV-A1A and A16 infections of HeLa or hAECN cells measured by dsRNA immunofluorescence.

(B) 25-HC does not affect the cell metabolic activity measured by resazurin assay. Values are means ± SD, n=4.

(C) EC_{50} values for 25-HC against HRV or CVB3 infections of HeLa or hAECN cells upon pretreatment of cells. Means ± SD, n=2.

(D) EC_{50} values for 25-HC added 1, 3 or 5 h pi. Means ± SD, n=2.

(E) RNAi against OSBP1 (pools of 4 individual siRNAs) compared to the negative control siRNA (all star) inhibits rhinovirus and to a lesser extent CVB3 infection of HeLa cells. Values are means ± SD, n=2.

(F) Western blots against OSBP1 from lysates of HeLa cells infected with HRV-A16 (MOI 50, 8 h), including blots against VP0, VP2 and GAPDH.

(G) Schematic depiction of OSBP1 containing a PH domain that binds PI4P and Arf1-GTP on Golgi membranes, an FFAT motif that binds VAP proteins on ER membranes, and an OSBP-related ligand-binding domain (ORD) that shuttles cholesterol and PI4P between membranes.

(H) Immunofluorescence analyses of FLAG-tagged OSBP1 or PH-domain lacking FLAG-OSBP1 (ΔPH FLAG-OSBP) expressed in HeLa cells infected with HRV-A1A or A16 (8 h). VP2 staining (green), FLAG-tagged OSBP1 (red) and nuclei (DAPI, blue). Scale bar: 10 µm.

(I) RNAi against VAP-B, Sac1 or PITP-b (pools of 4 individual siRNAs each) compared to the negative control siRNA (all star) inhibits HRV-A1A and A16 infection of HeLa cells (8 h). Values are means ± SD, n=2.

(J) Western blots against VAP-B, Sac1 and PITPb from lysates of HeLa cells infected with HRV-A16 (MOI 50, 8 h), including blots against VP0, VP2 and GAPDH.

Figure 6: The PI4K3b-OSBP1-Sac1-PITPb cycle is fueled by storage cholesterol and drives rhinovirus replication

(A) Model for Host factors and inhibitor profiling data for HRV replication (this study), including location of PI4Ks and OSBPL proteins (Balla, 2013; Carvou et al., 2010; Manna et al., 2013; Mesmin et al., 2013; Olkkonen and Li, 2013).

(B) Lipid counter-current flux for rhinovirus replication. 1) Tethering or activation of PI4K3b to Golgi membranes, by one or several viral membrane associated proteins, such as 2B or 3A. 2) Production of PI4P lipids on the Golgi. 3) Non-vesicular transport of PI4P from Golgi to ER and cholesterol from ER to Golgi through OSBP1. 4) Hydrolysis of cholesteryl-esters from LDs associated with ER (a) or late endosomes (b, c), and minor contribution from newly synthesized cholesterol (question mark, d). 5) Hydrolysis of PI4P to PI in the ER. 6) Transport of PI from ER to Golgi through the PI transfer protein PITP-b. 7) These events support viral RNA replication and involve RNA-dependent RNA polymerase $3C/D^{pol}$.

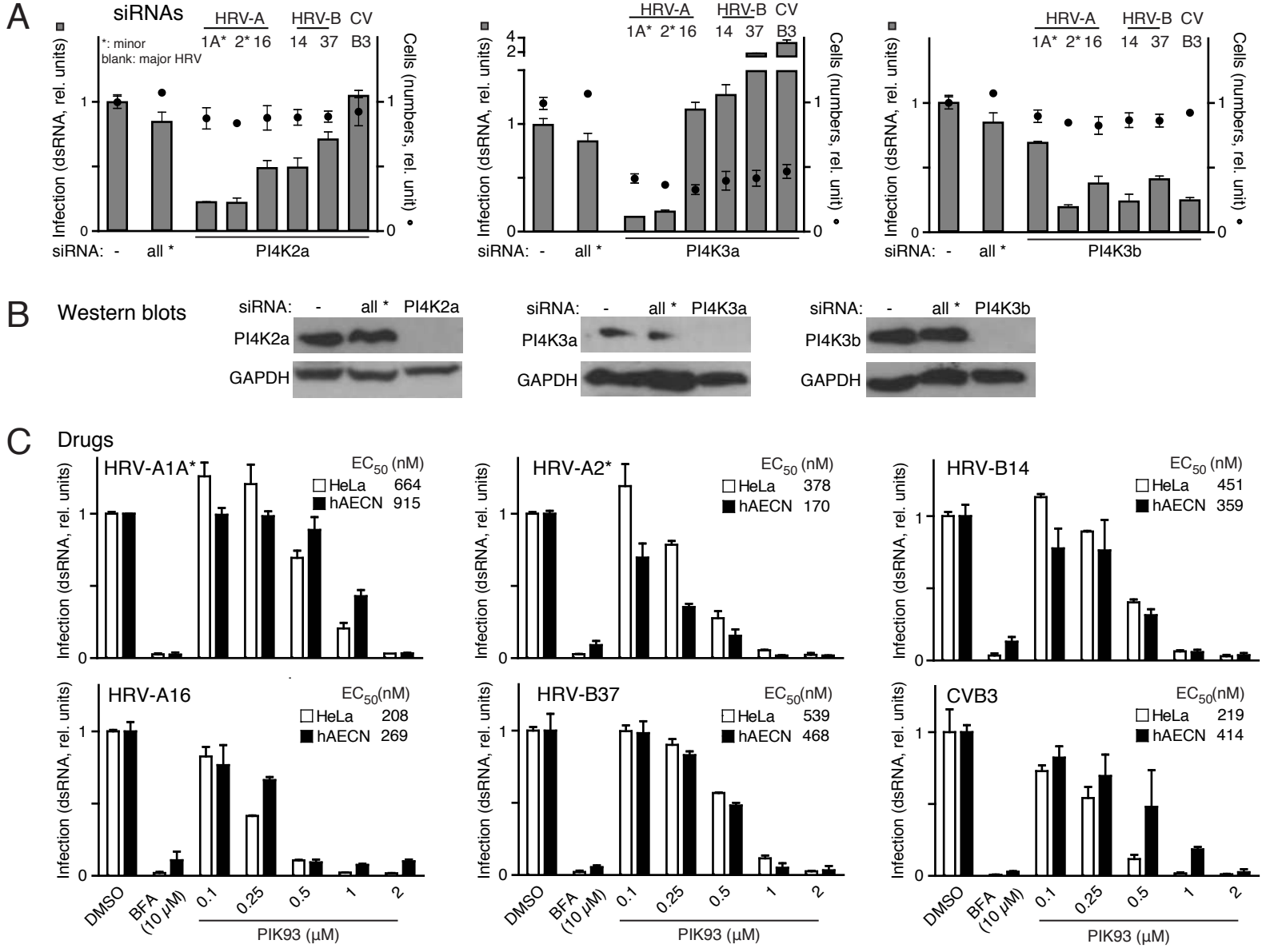
A
siRNAs
*: minor
blank: major HRV
HRV-A
HRV-B
CV
1A* 2* 16 14 37 B3
Infection (dsRNA, rel. units)
Cells (numbers, rel. unit)
siRNA: - all * PI4K2a
siRNA: - all * PI4K3a
siRNA: - all * PI4K3b
B
Western blots
siRNA: - all * PI4K2a
PI4K2a
GAPDH
siRNA: - all * PI4K3a
PI4K3a
GAPDH
siRNA: - all * PI4K3b
PI4K3b
GAPDH
C
Drugs
HRV-A1A*
EC50 (nM)
HeLa 664
hAECN 915
HRV-A2*
HeLa 378
hAECN 170
HRV-B14
HeLa 451
hAECN 359
HRV-A16
EC50(nM)
HeLa 208
hAECN 269
HRV-B37
HeLa 539
hAECN 468
CVB3
HeLa 219
hAECN 414
Infection (dsRNA, rel. units)
DMSO
BFA (10 μM)
0.1 0.25 0.5 1 2
PIK93 (μM)

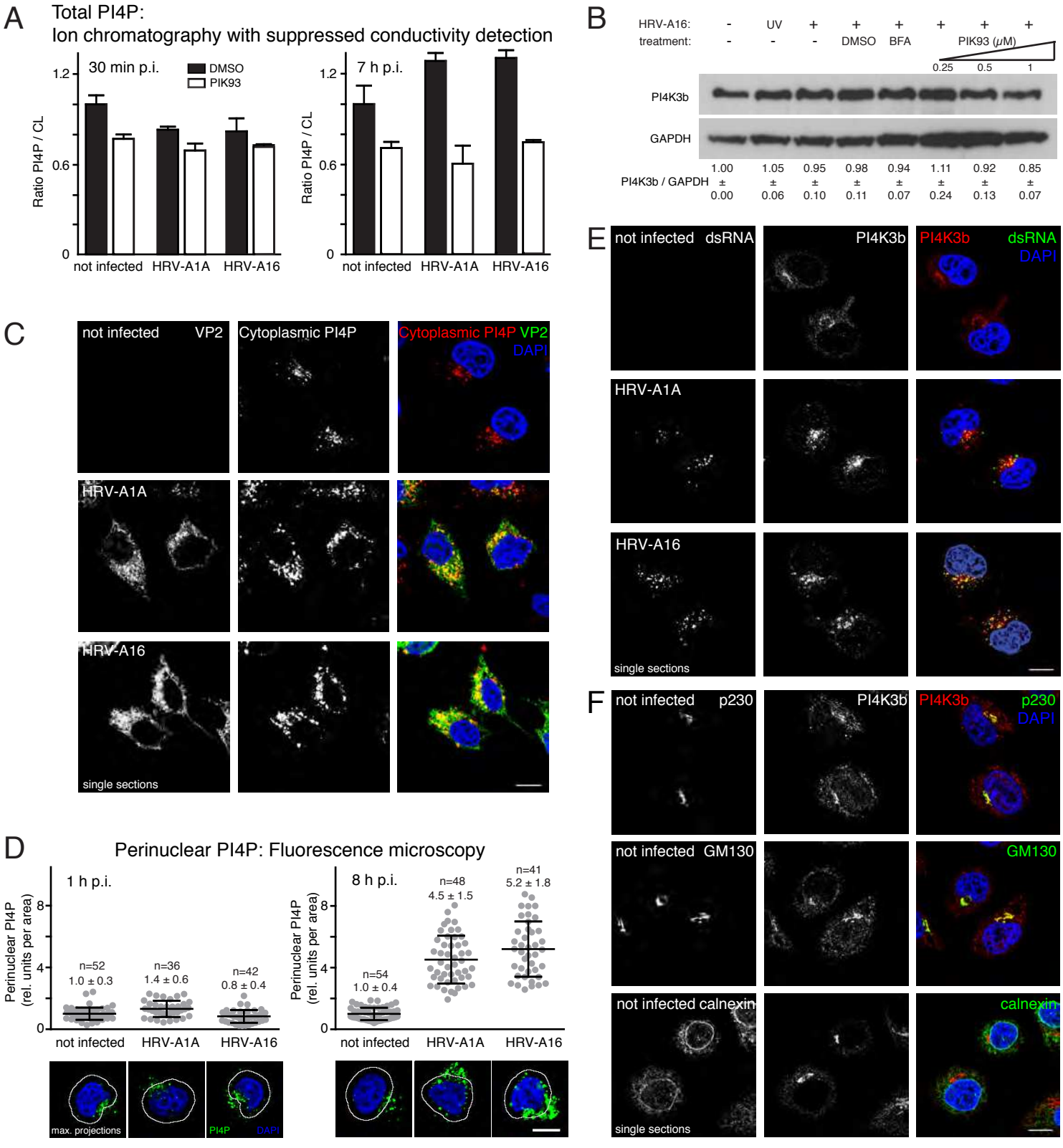
A
Total PI4P:
Ion chromatography with suppressed conductivity detection
30 min p.i.
DMSO
PIK93
Ratio PI4P / CL
1.2
0.6
0
not infected
HRV-A1A
HRV-A16
7 h p.i.
B
HRV-A16:
treatment:
DMSO
BFA
PIK93 (μM)
0.25
0.5
1
PI4K3b
GAPDH
PI4K3b / GAPDH
1.00 ± 0.00
1.05 ± 0.06
0.95 ± 0.10
0.98 ± 0.11
0.94 ± 0.07
1.11 ± 0.24
0.92 ± 0.13
0.85 ± 0.07
C
not infected
VP2
Cytoplasmic PI4P
Cytoplasmic PI4P VP2
DAPI
HRV-A1A
HRV-A16
single sections
D
Perinuclear PI4P: Fluorescence microscopy
1 h p.i.
8 h p.i.
Perinuclear PI4P
(rel. units per area)
n=52
1.0 ± 0.3
n=36
1.4 ± 0.6
n=42
0.8 ± 0.4
n=54
1.0 ± 0.4
n=48
4.5 ± 1.5
n=41
5.2 ± 1.8
max. projections
PI4P
DAPI
E
not infected
dsRNA
PI4K3b
PI4K3b
dsRNA
DAPI
HRV-A1A
HRV-A16
single sections
F
not infected
p230
PI4K3b
PI4K3b
p230
DAPI
not infected
GM130
GM130
not infected
calnexin
calnexin
single sections

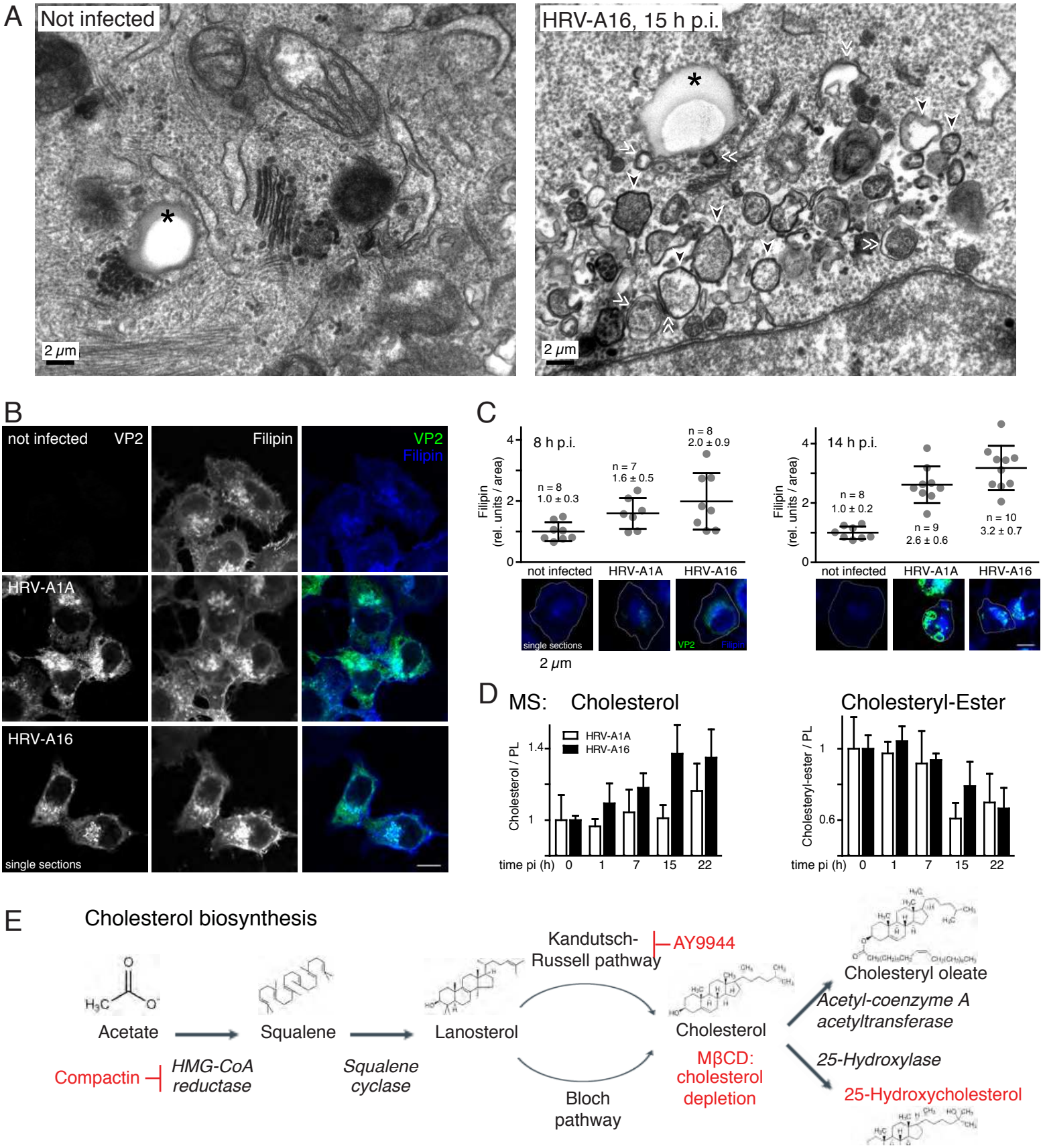
A
Not infected
HRV-A16, 15 h p.i.
2 μm
2 μm
B
not infected
VP2
Filipin
VP2
Filipin
HRV-A1A
HRV-A16
single sections
C
8 h p.i.
14 h p.i.
Filipin (rel. units / area)
n = 8
1.0 ± 0.3
n = 7
1.6 ± 0.5
n = 8
2.0 ± 0.9
n = 8
1.0 ± 0.2
n = 9
2.6 ± 0.6
n = 10
3.2 ± 0.7
not infected
HRV-A1A
HRV-A16
single sections
VP2
Filipin
2 μm
D
MS: Cholesterol
Cholesteryl-Ester
Cholesterol / PL
Cholesteryl-ester / PL
HRV-A1A
HRV-A16
time pi (h) 0 1 7 15 22
E
Cholesterol biosynthesis
Acetate
Squalene
Lanosterol
Cholesterol
Cholesteryl oleate
Kandutsch-Russell pathway
AY9944
Acetyl-coenzyme A acetyltransferase
Compactin
HMG-CoA reductase
Squalene cyclase
Bloch pathway
MβCD: cholesterol depletion
25-Hydroxylase
25-Hydroxycholesterol
F
Infection: Compounds added 1h pi
HRV-A1A
HRV-A16
8h
12h
10h
14h
Infection (VP2, rel. units)
no drug
25-HC (2 μM)
Compactin (10 μM)
AY9944 (10 μM)
G
Replication
HRV 5' UTR (rel. expression)
HRV-A1A
HRV-A16
no drug
25-HC (2 μM)
PIK93 (1 μM)
Compactin (10 μM)
AY9944 (10 μM)
H
Cholesterol biosynthesis
HMG-CoA reductase (rel. expression)
not infected
HRV-A1A
HRV-A16
no drug
25-HC (2 μM)
Compactin (10 μM)
AY9944 (10 μM)

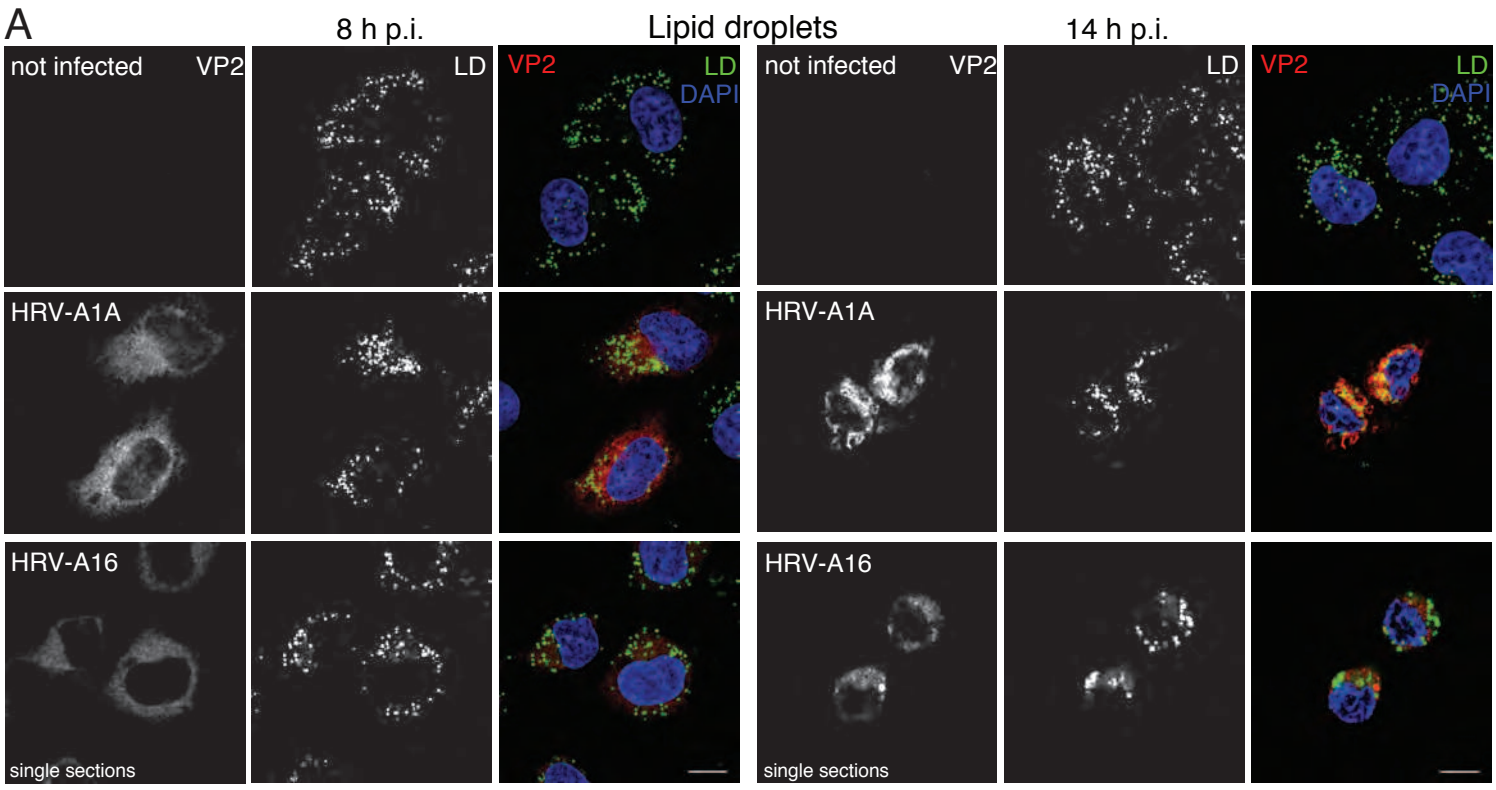

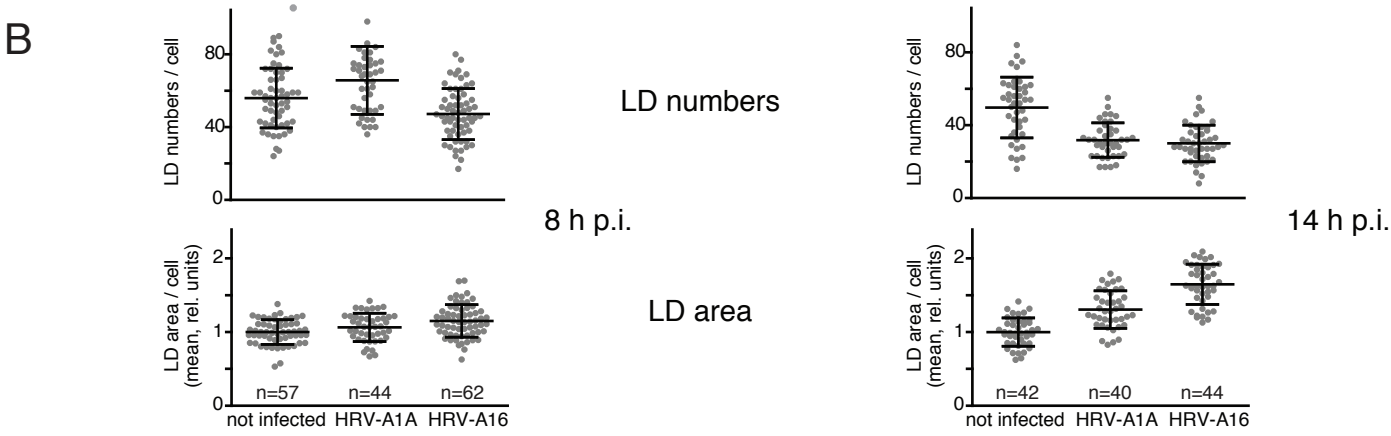

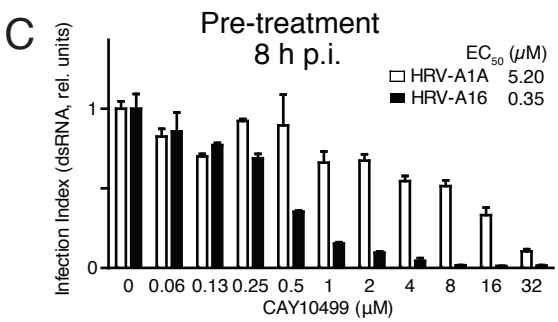

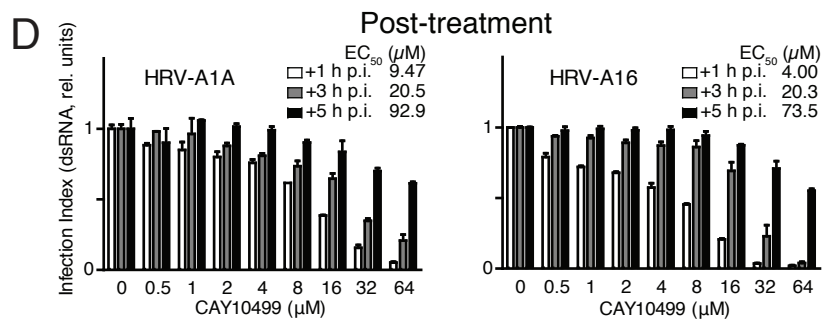

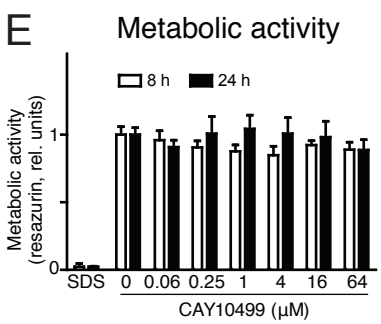

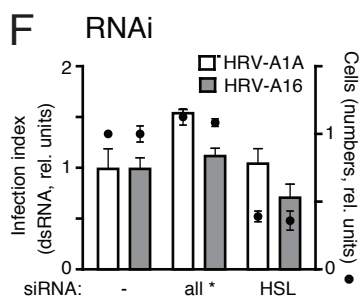

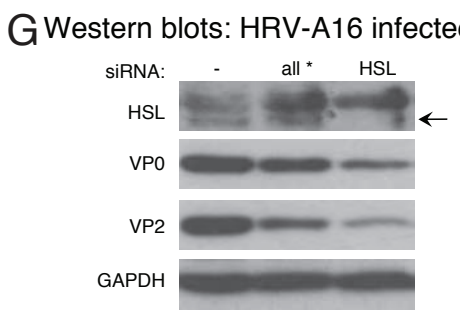

H RNA interference (+ denotes > 50% infection inhibition by immuno-fluorescence of dsRNA)

	OSBPL1	OSBPL2	OSBPL5	OSBPL6	OSBPL7	OSBPL8	OSBPL9	OSBPL10	OSBPL11
HRV-A1A*	+	+	+	+	+	+	+	+	+
HRV-A2*	+	-	+	+	-	-	+	+	+
HRV-A16	-	-	-	+	-	-	+	-	+
HRV-B14	-	-	-	-	-	+	+	-	+
HRV-B37	-	-	-	-	-	-	-	-	+
CVB3	-	-	-	-	-	-	-	-	-

*: minor blank: major HRV

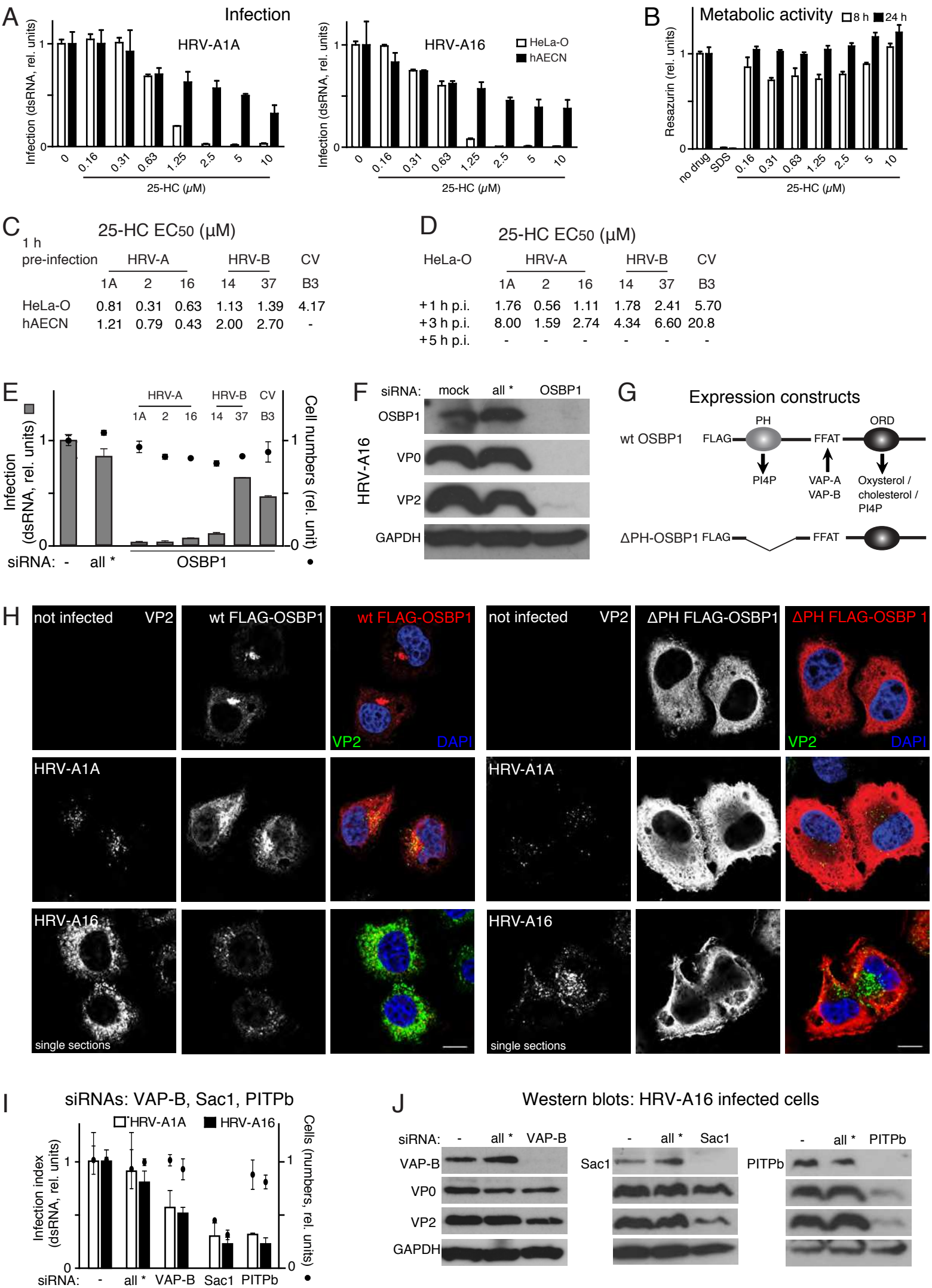
A
Infection
HRV-A1A
HRV-A16
HeLa-O
hAECN
Infection (dsRNA, rel. units)
25-HC (μM)
B
Metabolic activity
8 h
24 h
Resazurin (rel. units)
no drug
SDS
C
25-HC EC50 (μM)
1 h pre-infection
HRV-A
HRV-B
CV
1A 2 16 14 37 B3
HeLa-O 0.81 0.31 0.63 1.13 1.39 4.17
hAECN 1.21 0.79 0.43 2.00 2.70 -
D
25-HC EC50 (μM)
HeLa-O
+1 h p.i. 1.76 0.56 1.11 1.78 2.41 5.70
+3 h p.i. 8.00 1.59 2.74 4.34 6.60 20.8
+5 h p.i. - - - - - -
E
Infection (dsRNA, rel. units)
Cell numbers (rel. unit)
siRNA: - all * OSBP1
F
siRNA: mock all * OSBP1
HRV-A16
OSBP1
VP0
VP2
GAPDH
G
Expression constructs
wt OSBP1
FLAG
PH
FFAT
ORD
PI4P
VAP-A
VAP-B
Oxysterol / cholesterol / PI4P
ΔPH-OSBP1
H
not infected
VP2
wt FLAG-OSBP1
ΔPH FLAG-OSBP1
VP2
DAPI
HRV-A1A
HRV-A16
single sections
I
siRNAs: VAP-B, Sac1, PITPb
HRV-A1A
HRV-A16
Infection index (dsRNA, rel. units)
Cells (numbers, rel. units)
siRNA: - all * VAP-B Sac1 PITPb
J
Western blots: HRV-A16 infected cells
siRNA: - all * VAP-B
VAP-B
VP0
VP2
GAPDH
Sac1
PITPb

A

RNA interference

	PI4K2a	PI4K2b	PI4K3a	PI4K3b	OSBP1	VAP-B	Sac1	PITPb	HSL	OSBPL1	OSBPL2	OSBPL5	OSBPL9	OSBPL11
HRV-A1A	+++	-	+++	+	+++	++	++	++	-	++	++	++	++	+++
HRV-A2	+++	++	+++	+++	+++	+	n.d.	n.d.	+	+	-	++	++	+++
HRV-A16	++	+	-	++	+++	+	+++	+++	+	-	-	-	++	+++
HRV-B14	++	-	-	+++	+++	++	n.d.	n.d.	+	-	-	-	+	++
HRV-B37	+	+	-	++	+	-	n.d.	n.d.	-	-	-	-	+	++
CVB3	-	-	-	+++	++	-	n.d.	n.d.	-	-	-	-	-	-
Location	*Golgi/E*	*Golgi/E/PM*	*ER*	*Golgi*	*ER/Golgi*	*ER*	*ER*	*ER/Golgi*	*LD*	*ER/E*	*ER/LD*	*ER/E*	*ER/Golgi*	*Golgi/E*

Compounds

	PIK93	25-HC	CAY	MβCD	Compact	AY9944
HRV-A1A	++	++	+	++	-	-
HRV-A2	++	+++	+++	++	n.d.	n.d.
HRV-A16	+++	+++	+++	++	-	-
HRV-B14	++	++	++	-	n.d.	n.d.
HRV-B37	++	++	+	-	n.d.	n.d.
CVB3	++	+	-	-	n.d.	n.d.

E	*Endosome*
PM	*Plasma membrane*
ER	*Endoplasmic reticulum*
LD	*Lipid droplet*
CAY	*CAY10944*
MβCD	*Methyl-beta-cyclodextrin*
Compact	*Compactin*

Infection inhibition	
>75%	
50-75%	
25-50%	
-	< 25%
n.d. not determined	

B

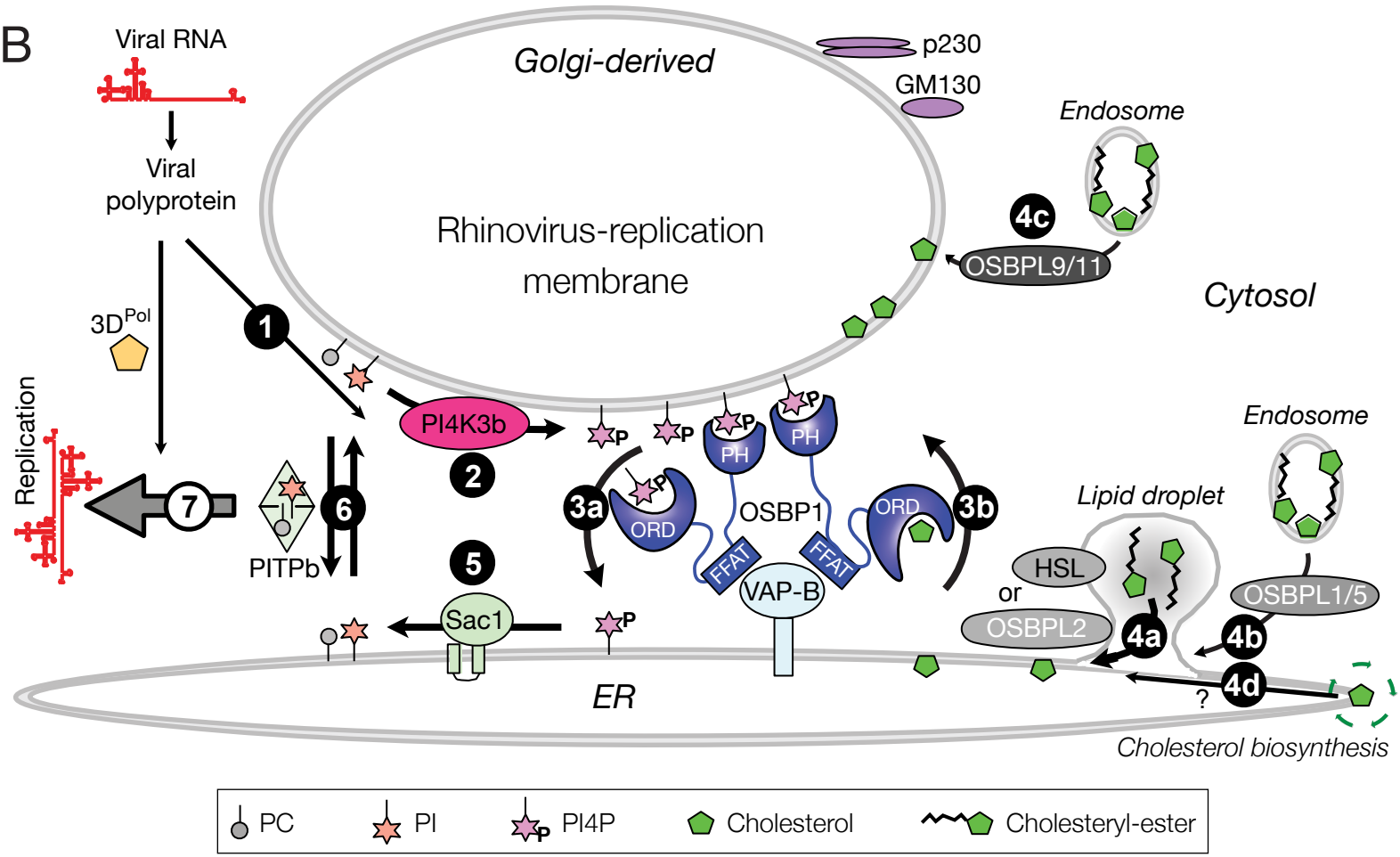

INVENTORY OF SUPPLEMENTS

SUPPLEMENTAL INFORMATION

Supplemental Data

Supplemental Figure S1: PI4K3b is required for replication of rhinoviruses in HeLa and human airway epithelial cells of nasal biopsies (related to Figure 1).

(A, C, E) Plate overviews of HeLa cells and human airway epithelial cells of nasal biopsies (hAECN) infected with HRV-A1A, A2, B14, A16, B37 or CVB3. Cells were stained for dsRNA (green) and nuclei (blue). Scale bar: 400 µM.

(B) HeLa cells were transfected with siRNAs targeting PI4K2b (pool of 4 individual siRNAs each, Dharmacon) or with the negative control siRNA (all star, all *). After 3 days, cells were infected with HRV-A1A, A2, B14, A16, B37 or CVB3 at MOI 20 for 8 h, and analyzed by high-throughput immunofluorescence microscopy. The ratio of infected cells to uninfected cells, and the number of total cells were determined and results normalized to the untreated control. Values: mean ± SD, n=2.

(D) HeLa cells were treated 1 h prior to infection with DMSO or PIK93, and infected with HRV-A1A or A16 at a MOI 20 for 8 h. Cells were stained for dsRNA (green) and PI4K3b (red). Nuclei were stained with DAPI (blue). Scale bar: 10 µm.

(F) HeLa cells were treated with DMSO, SDS (0.01%), pleconaril (Ple = 2.62 µM), bafilomycin A1 (Baf = 100 nM), brefeldin A (BFA = 10 µM) or PIK93 (as indicated) for 8 or 24 h. The metabolic cell activity was measured by resazurin (Jurgeit et al., 2012). Values: mean ± SD, n=4.

(G) HeLa cells were infected with HRV-A16 at a MOI 20 as indicated. Optical densities of HRV 5' UTR and GAPDH were measured upon semi-quantitative RT-PCR reactions. The signals from HRV 5' UTR were normalized to the respective GAPDH signal. Values: mean ± SD, n=3.

(H) HeLa cells were treated 1 h prior to infection with DMSO, brefeldin A (BFA = 10 µM) or PIK93 (at indicated concentrations). Cells were infected with HRV-A16 or UV-treated HRV-

A16 at a MOI of 50 for 8 h. Lysates were blotted against the viral proteins VP0 and VP2, and GAPDH.

(I) HeLa cells were treated 1 h prior to infection with DMSO, brefeldin A (BFA = 10 μM) or PIK93 (at indicated concentrations). Cells were infected with HRV-A1A (white bars) or HRV-A16 (black bars) at MOI 20 for 8 h. Optical densities of HRV 5' UTR and GAPDH were measured upon semi-quantitative rt-PCR. The HRV 5' UTR optical density was normalized to its respective GAPDH optical density. The EC_{50} was obtained by nonlinear regression of the data fitted to the variable-slope sigmoidal dose-response. Values: mean ± SD, n=3.

Note that both Western blots (H) and rt-PCR assays (I) were validated by BFA, and a UV-irradiated HRV-A16 inoculum. Results showed that PIK93 strongly attenuated the levels of VP2 (and VP0) and viral RNA in HeLa cells. As expected from RNA interference with PI4K3b, HRV-A1A was less sensitive to PIK93 in the rt-PCR assay than HRV-A16.

(J) HeLa cells were treated 1 h prior to infection or RNA transfection with DMSO, pleconaril (Ple = 2.62 μM), bafilomycin A1 (Baf = 100 nM), brefeldin A (BFA = 10 μM) or PIK93 (as indicated). Cells were infected with HRV-A1A or HRV-A16 at a MOI of 1 (white bars) or transfected with HRV-A1A or HRV-A16 viral RNA genome (black bars) for 18 h. By high-throughput immunofluorescence-based microscopy, the ratio of infected cells was calculated and normalized to the DMSO control. The EC_{50} was obtained by nonlinear regression of the data fitted to the variable-slope sigmoidal dose-response. Values: mean ± SD, n=2.

The data indicated that PI4K3b was involved at a post entry step of infection. Again, PIK93 had lesser effects on HRV-A1A than HRV-A16 RNA confirming that PI4K3b had a lesser role for A1A than for A16. Interestingly, HRV-A1A RNA transfection was less inhibited by PIK93 than A1A, suggesting that HRV-A1A entry renders the virus relatively insensitive to PIK93. Note that viral RNA transfections but not virus infections were always relatively insensitive to pleconaril and Baf, which block HRV-A1A or A16 infections (Jurgeit et al., 2012), indicating that the transfected RNA was free from infectious virus.

(K) HeLa cells were infected with HRV-A1A or HRV-A16 at MOI 20 for 8 h. At 1 h (white bars), 3 h (grey bars) or 5 h (black bars) post-infection, cells were treated with DMSO, brefeldin A (BFA = 10 μM) or PIK93 (at the indicated concentrations). By high-throughput immunofluorescence-based microscopy, the ratio of infected cells was calculated and normalized to the DMSO control. The EC_{50} was obtained by nonlinear regression of the data fitted to the variable-slope sigmoidal dose-response. Values: mean ± SD, n=2. The data showed that HRV-A1A and A16 were inhibited by PIK93 at or before 3 h pi, but much less at 5 h pi, similar to BFA. This also confirmed that the dsRNA assay measured RNA replication rather than incoming RNA.

(L) HeLa cells were infected with HRV-A1A or HRV-A16 at MOI 1 and PIK93 at 1 μM was added every 2 h. After 14 h, cells and medium were extracted and tittered on fresh HeLa cells. After 4 days, the $TCID_{50}$/ml was calculated using the Spearman-Karber method as described (Puntener et al., 2011; Spearman, 1908). The data show a half maximal time of virus inhibition by 1 μM PIK93 around 8 h pi. As HRVs start to replicate 3 to 4 h pi (Krenn et al., 2005), the data imply that PI4K3b does not affect steps upstream of viral replication, but is critical for RNA replication and gene expression.

(M) Dose dependent inhibition of HRV-A1A, A2, A16, B14, B37 and CVB3 infections of HeLa cells by GSK2998533A (GlaxoSmithKline, Infectious Disease R&D, North Carolina, USA) added prior to infection. EC_{50} values are indicated in nM. Note that EC_{50} values were all between 29.3 and 99.4 nM. Note that cell numbers were not affected up to 500 nM of the compound, suggesting low levels of toxicity.

(N) Inhibition profiles of HRV-A1A, A2, A16, B14, B37 and CVB3 infections of HeLa cells by GSK2998533A added 1, 3 or 5 h post infection. Note that EC_{50} values were below 200 nM if the compound was added before 3 h pi, and had no anti-viral efficacy if added 5 h pi. We conclude that PI4K3b is a key host factor for rhinovirus infections of HeLa and primary human nasal epithelial cells.

Supplemental Figure S1

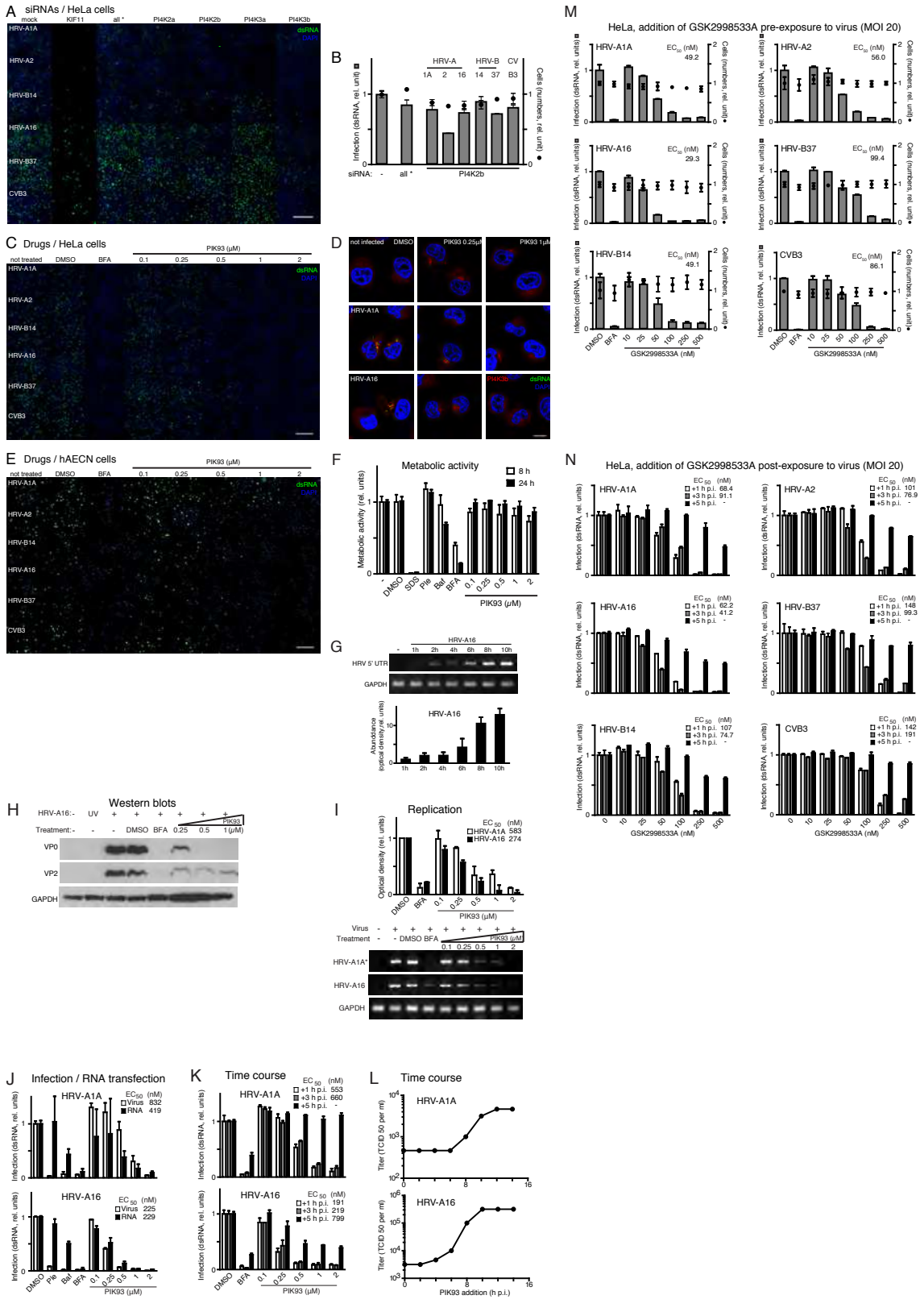

Supplemental Figure S2: HRV requires intact Golgi membranes to start replicating which are later rearranged (related to Figure 2).

(A, B, C, D) HeLa cells were infected with HRV-A1A or HRV-A16 at a MOI of 20 for 8 h. Cells were stained for VP2 (green) and host cell membrane markers (red) including p230 (C), GM130 (D), ERGIC-53 (E) and calnexin (F). Nuclei were stained with DAPI (blue). Scale bar: 10 µm.

(E) Non-infected HeLa cells were treated with DMSO, brefeldin A (BFA = 10 µM) or Exo2 (50 µM) for 8 h. Cells were stained for p230, GM130, ERGIC-53 or calnexin (green). Nuclei were stained with DAPI (blue). Scale bar: 10 µm.

(F) HeLa cells were infected with HRV-A1A or HRV-A16 at a MOI of 20 for 8 h. At 1 h (white bars), 3 h (grey bars) or 5 h (black bars) post-infection, cells were treated with DMSO, brefeldin A (BFA = 10 µM) or Exo2 (at the indicated concentrations). By high-throughput immunofluorescence-based microscopy, the ratio of infected cells was calculated and normalized to the DMSO control. The EC_{50} was obtained by nonlinear regression of the data fitted to the variable-slope sigmoidal dose-response. Values: mean ± SD, n=2.

Supplemental Figure S2

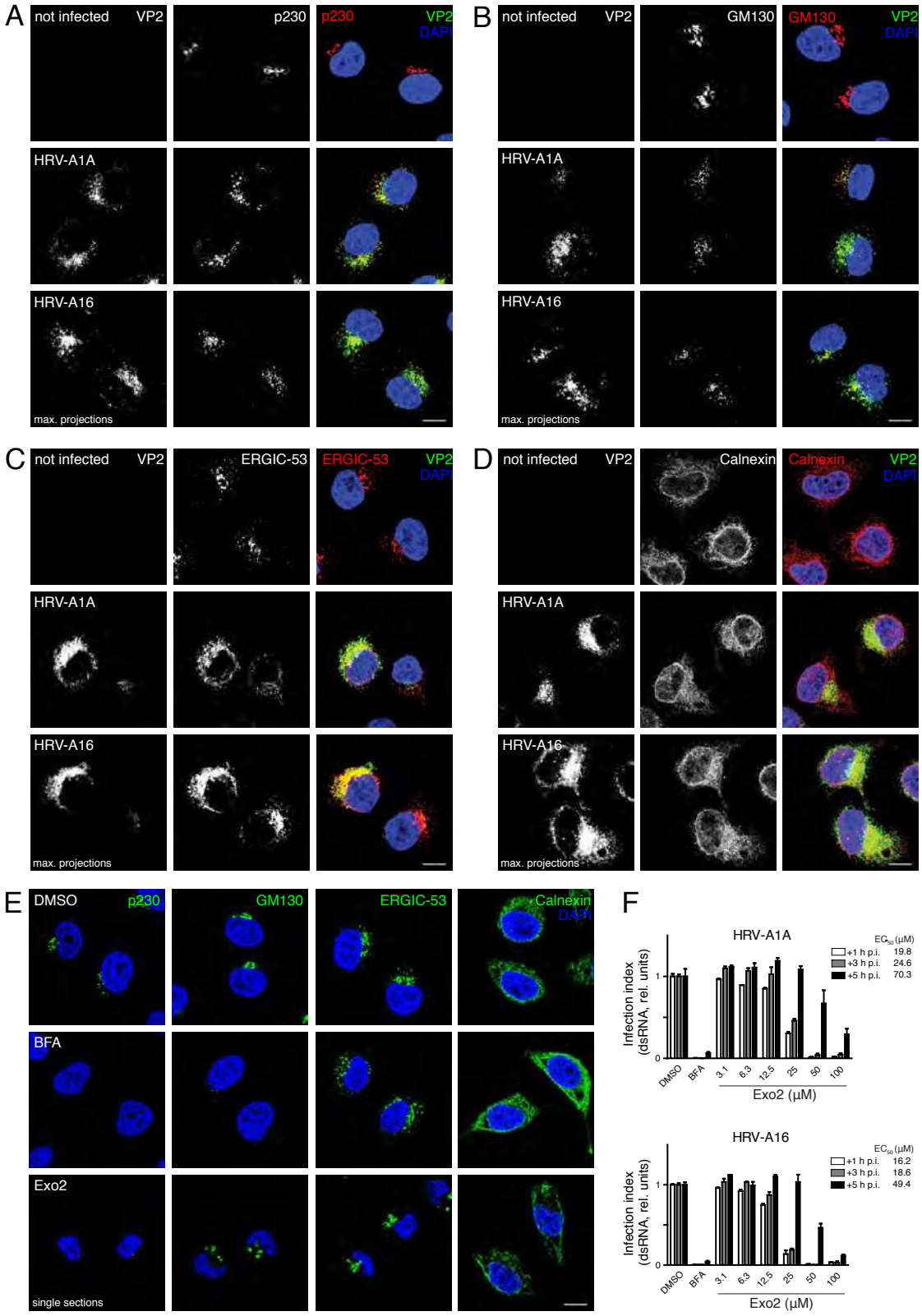

Supplemental Figure S3: Rhinovirus infection is reduced by 25-hydroxycholesterol but not inhibitors of cholesterol biosynthesis (related to Figure 3).

(A) Absolute amounts of cholesterol and cholesteryl-esters determined by mass spectrometry in HRV-A1A and HRV-A16 infected cells (MOI 50) at 1, 7, 15 or 22 h pi. Values: mean ± SD, n=3.

(B) HeLa cells were infected with HRV-A1A (left panel) or HRV-A16 (right panel) at a MOI of 20 for 8 h (white bars) or 14 h (black bars). After 1 h, cells were washed. At 2 h post-infection, cells were treated with PIK93, 25-hydroxycholesterol (25-HC), MbCD, compactin or AY9944 (at the indicated concentrations). By high-throughput immunofluorescence-based microscopy, the ratio of infected cells was calculated and normalized to the mock control. Values: mean ± SD, n=2.

(C) HeLa cells were treated with SDS (0.01%), MβCD, compactin or AY9944 (at the indicated concentrations) for 8 h and 24h. The cell metabolic activity was measured by adding resazurin. Values: mean ± SD, n=4.

Supplemental Figure S3

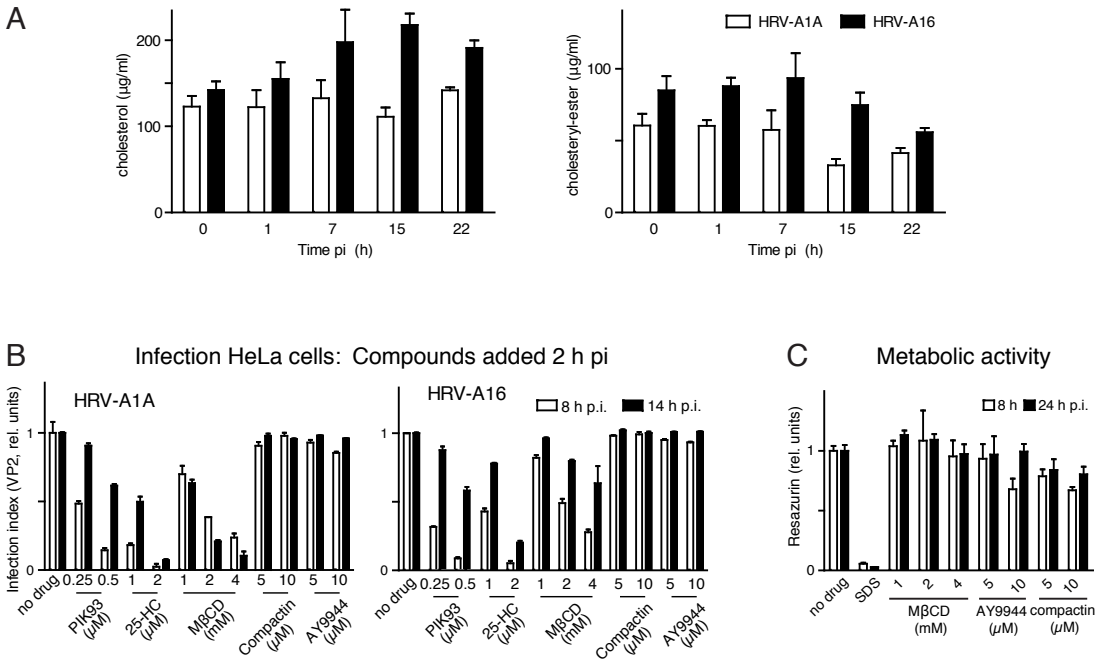

Supplemental Figure S4: RNAi against OSBPL proteins has differential effects on rhinovirus and CVB3 infections (related to Figure 4).

(A) Immunofluorescence of OSBPL9 and OSBPL11 in uninfected or HRV-A1A or A16 infected HeLa cells at MOI 20 8 h pi. Single confocal fluorescence microscopy midplane sections are shown with rabbit anti-OSBPL9 (Wyles and Ridgway, 2004), rabbit anti-OSBPL11 (Zhou et al., 2010), and mouse anti-dsRNA stainings (Jurgeit et al., 2010) and cell nuclei stained with diamidino-2-phenylindole (DAPI, blue).

(B) Expression profiling of OSBP1, OSBPL1, L2, L5, L9, L11 upon siRNA knock-down of the corresponding transcripts. Note the high degree of on target siRNA knock-down specificity achieved with pools of 4 siRNA per gene (Dharmacon).

(C) HeLa cells were treated with siRNAs (pools of 4 siRNA per gene, Dharmacon) as indicated, inoculated with HRV-A1A, A2, B14, A16, B37 and scored for infection using dsRNA immunofluorescence microscopy in high-throughout mode. Mock (uninfected, untreated) and all star (*) siRNA treated cells served as negative controls.

(D) Validation of HRV-A16 infection inhibition upon siRNA-mediated knock-down of OSBP1, OSBPL5, OSPBL9 and OSBPL11. The infection readout was by rt-PCR specific for the 5’ untranslated region (UTR) of genomic RNA.

Supplemental Figure S4

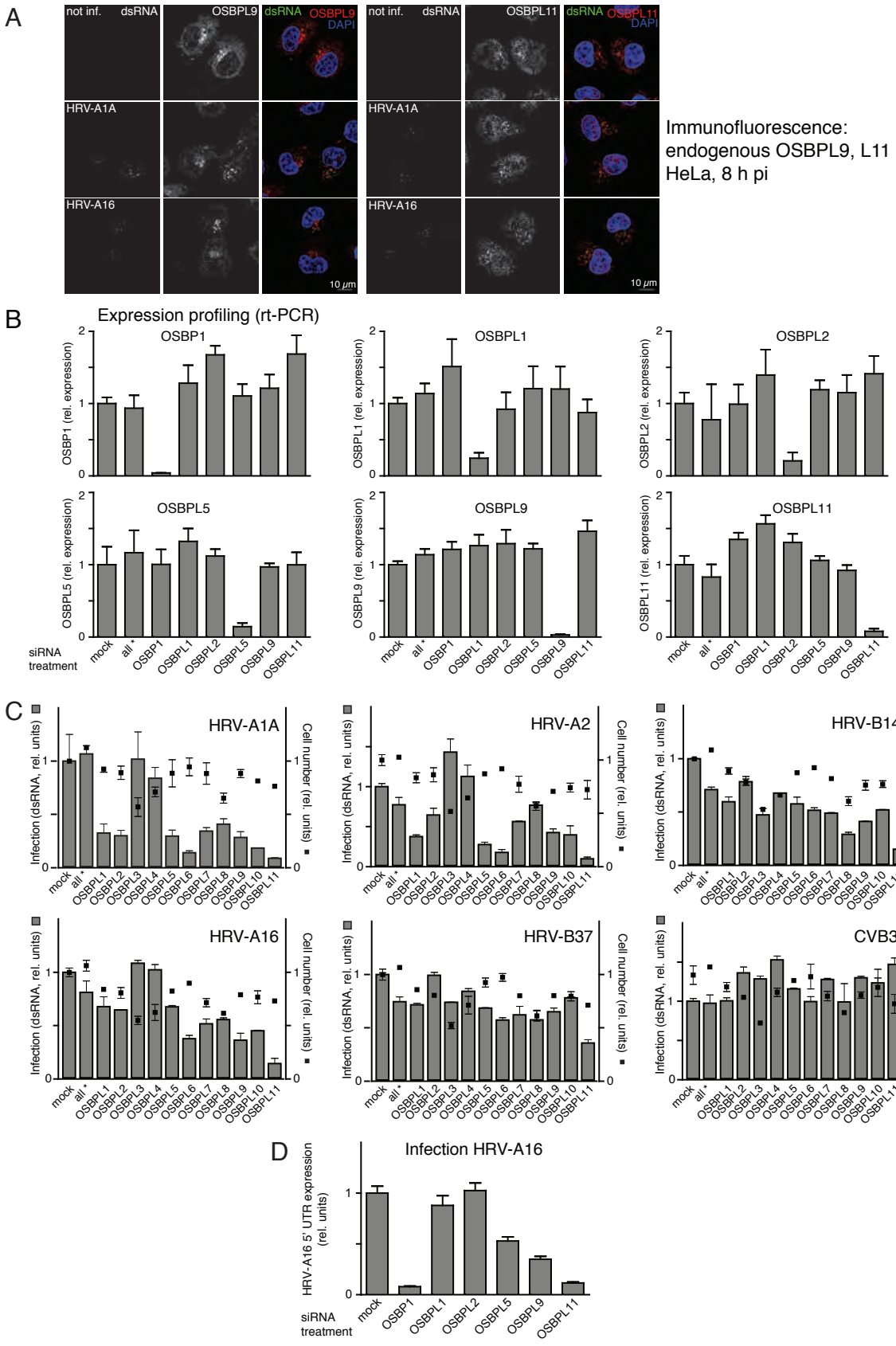

Supplemental Figure S5: 25-hydroxycholesterol blocks rhinovirus infection post entry by clustering OSBP1 at perinuclear sites (related to Figure 5).

(A) Non-infected HeLa cells were treated with 25-HC (at the indicated concentrations) for 8 h. Cells were stained for OSBP (green) and nuclei (blue). Scale bar: 10 µm.

(B, C, D) Plate overviews of Figure 5E (B), Figure 5A and 5C for HeLa cells (C), and Figure 5A and 5C for hAECN cells (D). Cells were stained for dsRNA (green) and nuclei (blue). Scale bar: 400 µM.

(E) HeLa cells were treated 1 h prior to infection with 25-HC (at the indicated concentrations). Cells were infected with HRV-A1A or HRV-A16 at a MOI of 20 for 8 h. Cells were stained for VP2 (green) and nuclei (blue). Scale bar: 10 µm.

(F) HeLa cells were treated 1 h prior to infection, or 1 h, 3 h or 5 h post-infection with 25-HC (at the indicated concentrations). Cells were infected with HRVs (HRV-A1A, HRV-A2, HRV-A16, HRV-B14 or HRV-B37) or CVB3 at a MOI of 20 for 8 h. By high-throughput immunofluorescence-based microscopy, the ratio of infected cells was calculated and normalized to the mock control. Values: mean ± SD, n=2.

Supplemental Figure S5

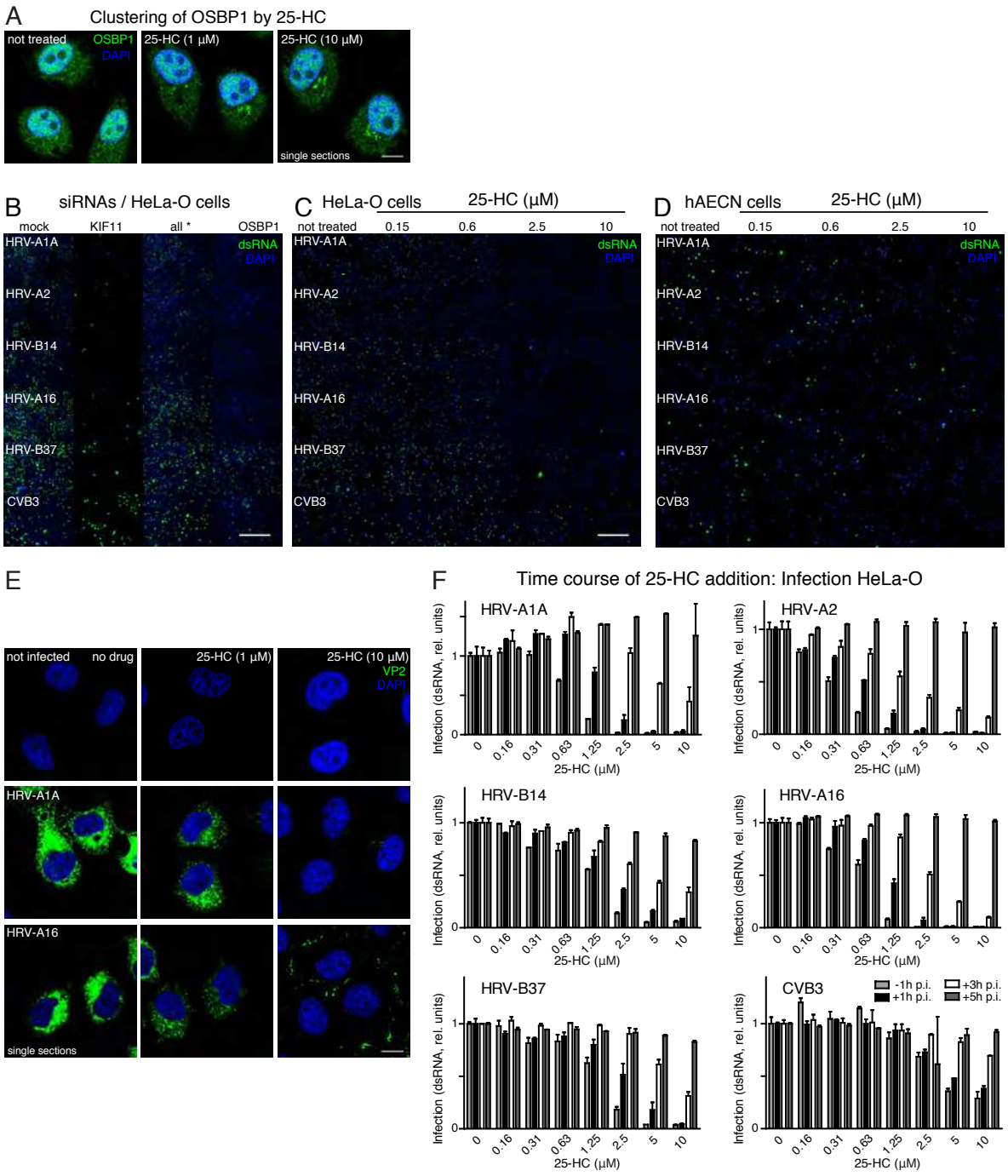

Supplemental Experimental Procedures

Chemicals, plasmids, antibodies and cell lines

The PIK43b inhibitor PIK93 was purchased from Selleck Chemicals, BFA from LC Laboratories, Baf, MβCD, filipin and 25-HC from Sigma, AY9944 from Tocris. Compactin was a kind gift from L. Rohrer (Institute of Clinical Chemistry, University Hospital Zurich, Switzerland), and LD540 from R. Klemm (Institute of Molecular Life Sciences, University of Zurich, Switzerland).

The plasmids FLAG-OSBP1_WT and FLAG-ΔPH OSBP1 were a gift from A. Siddiqui (Department of Medicine, University of California, USA). SMARTpool siGENOME siRNAs were purchased from Dharmacon.

Antibodies were obtained as follows: mouse monoclonal (Mab) 16-7 (W.M. Lee, Department of Pediatrics, School of Medicine and Public Health, University of Wisconsin, USA, used as in Jurgeit et al., 2010), Mab J2 (English & Scientific Consulting). Mabs against p230, GM130 and PI4K3b (BD Transduction Laboratories), Mab against ERGIC-53 and rabbit polyclonal antibody against calnexin (Stressgen), rabbit polyclonal antibody against PI4K3b (Millipore), rabbit polyclonal antibodies against PI4K3a and GAPDH (Cell Signaling), rabbit polyclonal antibody against OSBP1 (ProteinTech), rabbit polyclonal antibody against SAC1 (Abcam), Mab against PI4P (Echelon), rabbit polyclonal antibody against OSBPL9 from Dr. Neil Ridgway (Wyles and Ridgway, 2004), rabbit polyclonal antibody against OSBPL11 from Dr. Vesa Olkkonen (Zhou et al., 2010), Mab against PI4P were from Echelon Biosciences, and used as described (Hammond et al., 2009), rabbit polyclonal antibody against FLAG (Sigma), and Alexa Fluor-488 or -594 labeled secondary antibodies against mouse or rabbit IgG or IgM (Invitrogen). Mab 1C4 against PI4K2a was a gift from S. Minogue (Institute of Liver and Digestive Health, University College London, UK, Banerji et al., 2010), mab 1C1 against PITPb from S. Cockcroft (Department of Neuroscience, Physiology and Pharmacology, University College London, UK, Carvou et al., 2010).

HeLa cervical carcinoma cells strain Ohio (HeLa-O, from L. Kaiser; Central Laboratory of Virology, University Hospital Geneva, Switzerland) were cultured in Dulbecco's Modified

Eagle Medium (DMEM) supplemented with 10% heat-inactivated fetal bovine serum (FBS) and 1% L-glutamine.

Virus titration

HeLa-O cells were cultured overnight at 37°C in full medium, infected with purified HRV in infection medium and presence of inhibitor. At 14 h post-infection, cultures were collected and subjected to titrations by serial ten-fold dilutions in 96-well plates containing nearly confluent HeLa-O cells for 4 days at 33.5°C, when cells were fixed and stained with crystal violet. The median tissue culture infectious dose (TCID50) was calculated with the Spearman-Kaerber formula as described (Puntener et al., 2011).

Detailed protocol for lipid extraction and analyses

For phosphoinositide analysis by ion chromatography with suppressed conductivity detection (Nasuhoglu et al., 2002), HeLa-O cells were cultured in 10-cm dishes at 37°C in DMEM supplemented with 10% heat-inactivated FBS and 1% non-essential amino acids (NEA). Cells were treated 1 h prior to infection with PIK93, infected with purified HRV (MOI of 50) in DMEM supplemented with 2% FBS and 1% NEA at 37°C for either 30 min or 7 h. For extraction, all solutions and samples were kept on ice. Cells were scraped and suspended in 0.4 ml methanol:HCl (12 N) at 96:4, supplemented with 2 mM $AlCl_3$. After the addition of about 0.8 ml of chloroform, samples were vortexed for 1 min, sonicated for 10 min, supplemented with 0.4 ml distilled H_2O, and centrifuged for 2 min at 10,000 *g*. The lower phase was collected and transferred into new tubes containing methanol:oxalic acid (2 mM) at 1:0.9. Samples were vortexed for 1 min and centrifuged for 2 min at 10,000 *g*. The lower phase was collected and dried in a speed-vac. Extracted lipids were deacylated in 40% methylamine:distilled-H_2O:N-butanol:methanol (5:1:1.25:6.5) at 55°C under continuous shaking for 45 min and dried. Samples were washed twice by eliminating the upper phase after resuspension in 0.6 ml N-butanol:petroleum-ether:ethyl-formate (20:4:1) and 0.5 ml of H_2O, mixing and centrifugation at 10,000 *g* for 2 min. The dried samples were resuspended in milli-Q water. To separate and detect anionic phospholipid head

groups, anion-exchange HPLC with KOH gradients, followed by suppressed conductivity detection was used. The HPLC system and columns used were all from Dionex Corporation (Sunnyvale, CA). For all results presented, an ICS-3000 HPLC system was equipped with an Ionpac AS-11-HC 2x250 mm column and an AG11-HC 2x50mm guard column. An AS-3000 autosampler was used for sample injection. Sample volumes were 50 ml, and injection volumes were 10 ml. Each sample was injected 2 times and samples were analysed in triplicates. Before injection, the column was equilibrated with 10 mM KOH for 5 min, followed by 1.5 mM KOH for 2 min, followed by elution in gradients of (1) 1.5 to 4 mM KOH 0-7 min post injection, (2) from 4 to 16 mM 7-12 min post injection, (3) 16 to 86 mM KOH 12-30 min post injection, and (4) re-equilibration with 10 mM KOH. PI4P lipid levels were expressed as normalized to mitochondrial cardiolipin.

For cholesterol and cholesteryl-ester analyses, HeLa-O cells were cultured in 10 cm dishes at 37°C in DMEM supplemented with 10% heat-inactivated FBS and 1% NEA. Cells were treated with inhibitors, infected with purified HRVs (MOI 50) in DMEM supplemented with 2% FBS and 1% NEA at 37°C for 1, 7, 15 or 22 h. For the lipid extractions, all solutions and samples were kept on ice. Cells were scraped in PBS and pelleted, resuspended with 30 μl PBS, supplemented with chloroform:methanol (1:2), vortexed twice for 1 min and incubated on ice for 30 min. Chloroform (0.3 ml) and 0.2 ml 1 M KCl were added, and samples were vortexed twice for 30 sec, incubated on ice for 1 min and centrifuged at 9,000 *g* for 5 min. The lower phase was collected and dried in a speedvac, resuspended in 100 μl chloroform/methanol and diluted 1:1 with a 10 μg/ml d6-cholesterol standard (CDN Isotopes, Canada). 10 μl of sample were analyzed using an Agilent HPLC 1100 system (Agilent) coupled with an Applied AB Sciex 3200 QTrap mass spectrometer (AB Sciex, Foster City, CA). Separation between cholesterol and cholesteryl-esters was obtained using an Agilent Zorbax Eclipse XDB-C18 column (i.d. 4.6 mm × 150 mm), an 11 min isocratic elution with chloroform:methanol 1:1 (v/v) as the mobile phase at 0.5 ml/min. The LC–MS instrument was operated in the positive atmospheric pressure chemical ionization (APCI) mode. The MRM transitions 369/161 and 375/161 for cholesterol (or cholesteryl-esters) and d6-cholesterol after water loss were monitored, respectively. Cholesterol and cholesteryl-ester levels were shown as normalized to phospholipid levels.

Detailed protocols for interference and high-throughput infection

siRNAs (20 nM) were reverse transfected to HeLa-O cells in 96-well plates using serum-free Opti-MEM (Invitrogen) and Lipofectamine RNAiMAX (Invitrogen) according to the manufacturer's protocol. At 72 h post-transfection, cells were infected with purified HRVs or CV at MOI 20 in infection medium (DMEM supplemented with 0.2% BSA, 1% L-glutamine and 30 mM $MgCl_2$) at 33.5°C for 8 h. For pharmacological interference, cells were seeded in 96-well plates and cultured overnight at 37°C in full medium (HeLa-O) and in hAEC medium for hAECN cells. Cells were treated with compounds, infected with purified HRV or CV (MOI 20) at 33.5°C and analyzed 8 or 16 h pi. For entry by-pass assays, HeLa-O cells grown in 96-well plates in full medium at 37°C for 24 h, were treated with compounds, transfected with viral RNA extracted from purified viruses (TransIT-mRNA transfection kit, Mirus Bio, USA), grown for 18 h at 33.5°C, and scored for infection, upon fixation with 1/3 volume culture volume 16% paraformaldehyde (PFA) followed by permeabilization with 0.2% Triton X-100, and immunostaining with mabJ2 or anti-VP2 antibodies in PBS containing 1% BSA as described (Jurgeit et al., 2010). Images were acquired with an ImageXpress Micro microscope (Molecular Devices) in automated mode, using a CoolSNAP HQ 12bit gray scale camera (Roper Scientific) and 10x/NA 0.5 objective (Nikon), and analyzed with a custom written script in Matlab (MathWorks, Inc. Natick, MA, USA). Infection indexes (fraction of infected cells per total cell number) were plotted with GraphPad Prism software (GraphPad) as relative units. Typically, infections under normal conditions yielded 30-40% infected cells.

Western blots

For siRNA treatments, siRNAs were reverse transfected to HeLa-O cells at 37°C in 24-well plates at a final 20 nM concentration using serum-free Opti-MEM (Invitrogen) and Lipofectamine RNAiMAX (Invitrogen) according to the manufacturer's protocol. At 72 h post-transfection, cells were infected with HRV (MOI of 50) in infection medium for 8 h at 33.5°C. Alternatively, HeLa-O cells in 24-well plates and full medium were treated 1 h prior to infection with compounds as indicated, infected with HRVs (MOI of 50) in infection medium for 8 h at 33.5°C, lysed in NP-40 lysis buffer, and analyzed by Western blotting on

Hybond-P PVDF membranes (GE Healthcare) blocked in TBS-T buffer containing 5% milk for 1 h and primary antibodies by overnight incubation at 4°C, horseradish peroxidase-conjugated secondary antibodies at 1:5000 dilution and signal detection using ECL Plus (GE Healthcare).

Quantitative rt-PCR

HeLa-O cells grown in 6-well plates were treated with AY9944 or compactin for 16 h, or PIK93 or 25-HC for 1 h prior to infection with purified HRVs (MOI 20) in infection medium and incubated at 33.5°C for 8 h. Total RNA was extracted using mirVana miRNA Isolation Kit (Ambion) and cDNAs were obtained by reverse transcription using Transcriptor High Fidelity cDNA Synthesis Kit (Roche) according to the manufacturer's instructions. Sense (5'-GGA CCC CTT TGC TTA GAT GAA A-3') and antisense (5'-CCA CCA AGA CCT ATT GCT CTG-3') primers were used to amplify a HMG-CoA reductase cDNA fragment with SYBR Green PCR Master Mix (Applied Biosystems) using 7900HT Fast Real-Time PCR System (Applied Biosystems). Relative HMG-CoA reductase expression levels were calculated and normalized to TFRC, EEF and GAPDH expression levels. HRV expression was controlled using sense (5'-GTG AAG AGC CGC GTG TGC T-3') and antisense (5'-GCT GCA GGT TTA AGG TTA GCC-3') primers specific for HRV-A1A and HRV-A16 5' UTR. All quantitative reverse transcriptase PCR reactions were performed in triplicates, and no reverse-transcriptase controls were included.

siRNAs (20 nM) were reverse transfected to HeLa-O cells in 12-well plates using serum-free Opti-MEM (Invitrogen) and Lipofectamine RNAiMAX (Invitrogen) according to the manufacturer's protocol. At 72 h post-transfection, cells were infected with purified HRV-A16 at MOI 20 in infection medium (DMEM supplemented with 0.2% BSA, 1% L-glutamine and 30 mM MgCl2) at 33.5°C for 8 h. Total RNA was extracted using mirVana miRNA Isolation Kit (Ambion), and cDNAs were obtained by reverse transcription using Transcriptor High Fidelity cDNA Synthesis Kit (Roche) according to the manufacturer's instructions. Sense and antisense primers were synthesized according to (Zhou et al., 2012), and used to amplify a OSBP1, OSBPL1, OSBPL2, OSBPL5, OSBPL9 and OSBPL11 cDNA fragments with SYBR Green PCR Master Mix (Applied Biosystems) using 7900HT Fast Real-Time PCR System (Applied Biosystems). Relative expression levels

were calculated and normalized to TFRC, EEF and GAPDH expression levels. All quantitative reverse transcriptase PCR reactions were performed in triplicates, and samples without reverse-transcriptase included.

Semi-quantitative rt-PCR

HeLa-O cells were cultured overnight at 37°C in full medium, treated with compounds and infected with HRV (MOI 20) in infection medium for 8 h at 33.5°C. Total RNA was extracted using TRI reagent (Sigma) and cDNAs were obtained by reverse transcription using SuperScript III (Invitrogen) according to the manufacturer's instructions. cDNAs were amplified by PCR using Taq polymerase (Sigma) with specific sense (5'-CAA GCA CTT CTG TTT CCC C-3') and anti-sense (5'-GAA ACA CGG ACA CCC AAA GTA-3') primers for HRV 5' UTR. Cellular glyceraldehyde 3-phosphate dehydrogenase (GAPDH) mRNA from the same sample was used as an internal control for normalization using the sense (5'-AGC CTC AAG ATC ATC AGC AAT G-3') and anti-sense (5'-ATG GAC TGT GGT CAT GAG TCC TT-3') primers. The PCR amplification occurred as follows: pre-heating at 94°C for 2 min, denaturation at 94°C for 30 sec, annealing at 55°C for 30 sec, and extension at 68°C for 2 min. The cycle was conducted 35 times, followed by incubation at 68°C for 10 min. PCR products were separated by electrophoresis (2% agarose gel), imaged, and quantified by ImageJ (National Institutes of Health) with normalization to the corresponding mean intensity signal from GAPDH.

Supplemental References

Banerji, S., Ngo, M., Lane, C.F., Robinson, C.A., Minogue, S., and Ridgway, N.D. (2010). Oxysterol binding protein-dependent activation of sphingomyelin synthesis in the golgi apparatus requires phosphatidylinositol 4-kinase IIalpha. Mol Biol Cell *21*, 4141-4150.

Carvou, N., Holic, R., Li, M., Futter, C., Skippen, A., and Cockcroft, S. (2010). Phosphatidylinositol- and phosphatidylcholine-transfer activity of PITPbeta is essential for COPI-mediated retrograde transport from the Golgi to the endoplasmic reticulum. J Cell Sci *123*, 1262-1273.

Hammond, G.R., Schiavo, G., and Irvine, R.F. (2009). Immunocytochemical techniques reveal multiple, distinct cellular pools of PtdIns4P and PtdIns(4,5)P(2). Biochem J *422*, 23-35.

Jurgeit, A., McDowell, R., Moese, S., Meldrum, E., Schwendener, R., and Greber, U.F. (2012). Niclosamide is a proton carrier and targets acidic endosomes with broad antiviral effects. PLoS Pathog *8*, e1002976; 1002910.1001371/journal.ppat.1002976.

Jurgeit, A., Moese, S., Roulin, P., Dorsch, A., Lotzerich, M., Lee, W.M., and Greber, U.F. (2010). An RNA replication-center assay for high content image-based quantifications of human rhinovirus and coxsackievirus infections. Virol J *7*, 264.

Krenn, B.M., Holzer, B., Gaudernak, E., Triendl, A., van Kuppeveld, F.J., and Seipelt, J. (2005). Inhibition of polyprotein processing and RNA replication of human rhinovirus by pyrrolidine dithiocarbamate involves metal ions. J Virol *79*, 13892-13899.

Nasuhoglu, C., Feng, S., Mao, J., Yamamoto, M., Yin, H.L., Earnest, S., Barylko, B., Albanesi, J.P., and Hilgemann, D.W. (2002). Nonradioactive analysis of phosphatidylinositides and other anionic phospholipids by anion-exchange high-performance liquid chromatography with suppressed conductivity detection. Anal Biochem *301*, 243-254.

Puntener, D., Engelke, M.F., Ruzsics, Z., Strunze, S., Wilhelm, C., and Greber, U.F. (2011). Stepwise loss of fluorescent core protein V from human adenovirus during entry into cells. J Virol *85*, 481-496.

Spearman, C. (1908). The Method of 'Right and Wrong Cases' (Constant Stimuli) without Gauss' Formulae. Brit J Psychology *2*, 227-442.

Wyles, J.P., and Ridgway, N.D. (2004). VAMP-associated protein-A regulates partitioning of oxysterol-binding protein-related protein-9 between the endoplasmic reticulum and Golgi apparatus. Exp Cell Res *297*, 533-547.

Zhou, Y., Li, S., Mayranpaa, M.I., Zhong, W., Back, N., Yan, D., and Olkkonen, V.M. (2010). OSBP-related protein 11 (ORP11) dimerizes with ORP9 and localizes at the Golgi-late endosome interface. Exp Cell Res *316*, 3304-3316.

Zhou, Y., Robciuc, M.R., Wabitsch, M., Juuti, A., Leivonen, M., Ehnholm, C., Yki-Jarvinen, H., and Olkkonen, V.M. (2012). OSBP-related proteins (ORPs) in human adipose depots and cultured adipocytes: evidence for impacts on the adipocyte phenotype. PLoS ONE *7*, e45352.